# Timing of Pleistocene glaciations in the High Atlas, Morocco: new 10Be and 36Cl exposure ages

**DOI:**
10.1016/j.quascirev.2017.11.015

**Document Version**
Accepted author manuscript

# Timing of Pleistocene glaciations in the High Atlas, Morocco: new $^{10}$Be and $^{36}$Cl exposure ages

Philip D. Hughes[1], David Fink[2], Ángel Rodés[3], Cassandra R. Fenton[3, 4] Toshiyuki Fujioka[2]

*[1] Geography, School of Environment and Development, The University of Manchester, Manchester, M13 9PL, England, UK.*

*[2] Australian Nuclear Science and Technology Organisation, PMB1, Menai, NSW 2234, Australia.*

*[3]NERC Cosmogenic Isotope Analysis Facility, SUERC, Scottish Enterprise Technology Park, Rankine Avenue, East Kilbride, G75 0QF, Scotland, UK.*

*[4] Colorado Mesa University, 1100 North Ave, Grand Junction, CO USA 81501*

**ABSTRACT: This paper presents data from 42 new samples yielding Late Pleistocene cosmogenic $^{10}$Be and $^{36}$Cl exposure ages of moraine boulders across a series of glaciated valleys in the Toubkal Massif (4167 m a.s.l.), High Atlas, Morocco. This represents the first comprehensive Pleistocene glacial chronology in North Africa and one of the largest datasets from the Mediterranean region. The timing of these glacier advances has major implications for understanding the influence of Atlantic depressions on moisture supply to North Africa and the Mediterranean basin during the Pleistocene. The oldest and lowest moraines which span elevations from ~1900-2400 m a.s.l. indicate that the maximum glacier advance occurred from MIS 5 to 3 with a combined mean $^{10}$Be and $^{36}$Cl age of 50.2 ± 19.5 ka (1 SD; n=12, 7 outliers). The next moraine units up-valley at higher elevations (~2200-2600 m a.s.l.) yielded exposure ages close to the global Last Glacial Maximum (LGM) with a combined mean $^{10}$Be and $^{36}$Cl age of 22.0 ± 4.9 ka (1 SD; n=9, 7 outliers). The youngest exposure ages are from moraines that were emplaced during the Younger Dryas with a combined mean $^{10}$Be and $^{36}$Cl age of 12.3 ± 0.9 ka (1 SD; n=7, no outliers) and are found in cirques at the highest elevations ranging from ~2900-3300 m a.s.l. From moraines predating the Younger Dryas, a large number of young outliers are spread evenly between 6 to 13 ka suggesting a continuing process of exhumation or repositioning of boulders during the early to mid-Holocene. This attests to active seismic processes and possibly intense erosion during this period.**

## 1. Introduction

There is more than a century-long history of glacial research in the Atlas Mountains, Morocco. Some of the earliest observations of glacial features are reported in '*Journal of a tour in Marocco and the Great Atlas*' by the English writers Hooker and Ball in 1878 and also by Thompson in 1899. In 1922, Frödin reported on glacial deposits as low as 500 m altitude near Marrakech; however, these deposits were subsequently re-interpreted as fluvial in origin by De Martonne (1924) who did not find any evidence of glaciation in lower valleys. De Martonne (1924) and Célérier and Charton (1922) reported glacial deposits in the headwaters of the Imenane and Rheraia Valleys on the northern slopes of the Toubkal massif (Figure 1). Dresch (1941) studied the geology of the entire Toubkal massif from Anrhemer (3942 m a.s.l.) in the northeast to Ouanoukrim (4089 m a.s.l.) in the southwest, and commented on the glacial geomorphology of the area. On the northern slopes of Aksoual (3912 m a.s.l.), De Martonne (1924) observed former glaciers had extended to 2000 m a.s.l. and that the snowline was situated at ~2800 m a.s.l. However, for the wider Toubkal Massif Dresch (1941, p. 622) argued that Pleistocene snowlines were situated at *c.* 3600-3700 m a.s.l. Later papers by German researchers Heybrock (1953) and Mensching (1953) confirmed the presence of glacial deposits in the Toubkal Massif. Studies by Messerli (1967), Messerli and Winiger (1980), Chardon and Riser (1982) provided some more insight into the detail of glaciation in the Toubkal area and this was followed up for the wider Atlas Mountains by Hughes et al. (2004) and Hughes et al. (2011a). A more recent survey on the Tazaghart and Iouzagner areas 5-10 km to the west of Toubkal have revealed geomorphological and sedimentological evidence for extensive plateau ice fields and a series of later smaller glacier phases, although these features are undated (Hannah et al. 2016).

In the Toubkal area, glacial features are often closely associated with mass-movement deposits. For example, Célérier and Charton (1923) suggested that a landslide dammed the lake of Lac d'Infi, on the southern slopes of Toubkal, as a result of glacier retreat up the valley. Neltner (1938) also considered Lac d'Infi to be dammed by a huge landslide. Another large rock accumulation at Arroumd in the upper reaches of the Rheraia valley in the Toubkal area, has been interpreted as a moraine (Hooker and Ball, 1878, p. 199), a rock glacier (Dresch, 1941; Mensching, 1953; Chardon and Riser, 1981), and a rock avalanche deposit (Hughes et al. 2011a). In the most recent research, cosmogenic $^{10}$Be exposure dating showed that the rock debris in this valley is mid Holocene in age and was formed by a massive rock avalanche, with seismic activity the likely trigger (Hughes et al., 2014). Nevertheless, there is also clear evidence of glaciation in this valley and Hughes et al. (2014) suggested that glaciers had over-steepened the backwall cliffs making them more prone to collapse.

Elsewhere in Morocco, glacial features have been described in the limestone High Atlas around Irhil M'Goun (Dresch 1949; Wiche 1953), the Middle Atlas (Dresch and Raynal 1953; Raynal et al. 1956; Awad 1963) and the Rif (Mensching 1960). In a review of the glacial record in Morocco, Awad (1963) identified evidence for glacial traces (including rock glaciers) during three main phases. In Moroccan continental chronostratigraphy the last glaciation is equated with the Soltanien Stage (Awad 1963, after Choubert *et al*. 1956) and is equivalent to the Würmian Stage in Alpine stratigraphy (Lefèvre and Raynal 2002). Awad (1963) correlated earlier glacial deposits with Middle Pleistocene cold stages such as the Tensiftien (Rissian; MIS 6) and earlier cold stages in the Moroccan stratigraphy. The High Atlas is a key physiographic barrier between the Atlantic Ocean, Sahara Desert and the Mediterranean and hence understanding the timing of glaciations in these mountains is a pre-requisite toward understanding Pleistocene environmental change in North Africa and also human evolution (Blome et al. 2012). The significance of glaciation in the High Atlas highlights the pressing need for more comprehensive dating of the glacial record.

The aim of this paper is to re-assess the timing and extent of Pleistocene glaciation from 9 valleys across the Toubkal Massif of the High Atlas, Morocco. Given that the last major geomorphological investigations were published by Dresch (1941) and Mensching (1953), there is a need to revise these seminal works in the light of more than 50 years of development in the fields of geomorphology and Quaternary science, especially in the application and availability of new geochronological techniques. This paper presents 1) new mapping for the geomorphological evidence of glaciation across the northern escarpment of the Marrakesh High Atlas, namely the slopes of Adrar el Hajj (3129 m a.s.l.; also known as Adra Adj on some maps), Aksoual (3912 m a.s.l.) Bou Iguenouane (3877m a.s.l.), and Toubkal (4167 m a.s.l.), and 2) the first radiometric based geochronological determination of glacial phases using $^{10}$Be and $^{36}$Cl exposure dating.

**2. Study Area**

The High Atlas near Marrakesh (c. 31.1°N, 7.9°W) contains the highest peaks of the Atlas chain, culminating at Jebel Toubkal. The mountains of this area are formed predominantly in Precambrian volcanic rocks (Figure 2). The upper slopes of the valleys and all the summits of the Toubkal massif are made of stacked basaltic flows whilst the lower parts of the massif, below 3500 m a.s.l., are formed in rhyolite, dacites, ignimbrites and andesites (Pouclet et al. 2007). The cliffs of the mountains in this area are over 2000 m high and expose a complex suite of extrusive volcanics. Consequently, the moraine boulders in these valleys have a very diverse range of extrusive volcanic lithologies. Some of the volcanic rocks contain quartz phenocrysts and quartz veins, whilst others have very limited quartz. Plutonic rocks are also present, though not common

in the glaciated headwaters, and consist of various grades of granites and diorites. Triassic sandstones and Cambrian limestones are present locally (Figure 2), although again these lithologies have not been subject to glaciation.

The area is tectonically active with numerous major faults. The most significant in the study area is the Tizi n'Test Fault which runs through several of the studied valleys, including Azib Mzik, Tamatert and the Imenane Valley (Delcaillau et al., 2010; 2011). The High Atlas are unusual in that they do not display evidence of significant crustal thickening. The crust is ~15 km thinner than would normally be expected for mountains reaching 4000 m in elevation (Miller and Becker 2014). A Plio-Quaternary uplift event has been determined using river profiles, which has been linked with the convective removal of the lithospheric root of the Atlas Mountains resulting in the anomalously high topography observed today (Boulton et al., 2017).

No glaciers exist today in the High Atlas. However semi-permanent snow fields do exist, the most famous being the *Névé Permanent* below the northern cliffs of the Tazaghart plateau. This site is likely to have been a true glacier in the Little Ice Age and moraines enclose the lower parts of the site (Hughes, 2014; Hannah et al. 2016). It is also possible that small patches of permafrost exist in sheltered shaded localities (Vieira et al. 2017). For example, Chardon and Riser (1981) identified a potential active rock glacier in the western cirque of Toubkal at an altitude of 3700-4000 m a.s.l.

The present-day annual temperature range at nearby Marrakech (484 m a.s.l.) is 16.1°C (mean annual 19.6°C; July 28.3°C and January 12.2°C) (World Meteorological Organisation, 1998). When temperatures are extrapolated using a lapse rate of 0.6°C per 100 m, the mean annual temperature at 4000 m a.s.l. is about -1.6°C (July 7.1°C, January -9.0°C). In the Aït Mizane valley draining the north side of Toubkal mean annual precipitation for the period 1949-50 to 1963-64 was 837.3 mm at the Neltner Refuge (3200 m a.s.l.) and 514.6 mm at Arroumd (1900 m) (Messerli 1967, p. 183).

## 3. Methods

### *3.1. Glacial geomorphology*

The glacial geomorphology of the Toubkal Massif was mapped in the field between 2007 and 2013 using 1:50,000 topographic base maps (Orientazion, 2006). Satellite imagery (GoogleEarth) was used to help target field exploration and improve the accuracy of the field mapping. Glacial landforms were mapped and subdivided using morpho-lithostratigraphy. This approach employs

morphological and lithological criteria to define, subdivide and correlate landforms (Hughes, 2010). A strict separation was maintained between field descriptions and landform interpretations. This was especially important since the same landforms in this area have been assigned contrasting geomorphologies by different authors, such as either rock avalanche, fluvial, periglacial or glacial deposits, or even as a combination of these. Lithological properties of landforms were assessed at both the surface and at section exposures using routine clast characteristics (e.g., size, shape, roundness, fabric, presence/absence of striae). The geomorphological observations were divided into three separate mountain-valley regions that during the last glacial cycle were glacially modified areas: Region 1: Aksoual-Bou Iguenouane; Region 2: Adrar el Hajj, and; Region 3: Toubkal. Valley morphometry for the nine glaciated valleys sampled for $^{10}$Be is given in Table 1.

*3.2. Geochronology*

Samples for cosmogenic $^{10}$Be (n = 24) and $^{36}$Cl (n = 18) analyses were taken from the upper exposed surface of 38 moraine boulders and from 4 glacially-modified bedrock outcrops. The largest boulders, embedded within moraine crests were targeted to minimise potential toppling and exhumation. Subrounded/subangular erratic boulders (sometimes with striations) were also preferred where possible as these have undergone abrasion and are likely to have been transported sub-glacially over significant distances, reducing the contribution of of inheritance to the post-depositional inventory of $^{10}$Be during sub aerial exposure**.** The variety in lithology and limited distribution of quartz required sampling andesites and basalts for $^{36}$Cl but where quartz veins were available and sufficient, preference was given to sampling for $^{10}$Be. No samples or same surfaces were analysed using both $^{10}$Be and $^{36}$Cl. Rock densities were measured in the laboratory with most conforming to expected values for quartz (~2.6 to 2.8 g/cm$^3$). The area contains some unusually dense minerals including barytes (densities up to 4.4 g/cm$^3$) and some quartz veins were dense (up to 3.41 g/cm$^3$). Topographic shielding was measured in the field using a compass and an abney level with shielding values calculated as described in Dunne et al. (1999). Details of sample locations, rock type and field setting are provided in Table 2.

*3.2.1. $^{10}$Be Analysis*

Twelve $^{10}$Be samples were prepared for AMS measurement at the Cosmogenic Geochemistry Laboratories at the Australian Nuclear Science and Technology Organisation (ANSTO) and 12 $^{10}$Be samples were prepared at the Cosmogenic Isotope Analysis Facility at the Scottish Universities Environmental Research Centre (SUERC). All results pertaining to the $^{10}$Be AMS analyses are provided in Table 3.

ANSTO samples were processed and measured following methods reported in Child et al., (2000). Fink et al., (2000) and Mifsud et al., (2013). Further details pertaining to chemistry processing samples of similar andesitic and basaltic lithologies are given in Hughes et al. (2014) for dating a rock avalanche site in the same area of Morocco. AMS targets were measured for $^{10}$Be at the ANTARES AMS Facility at ANSTO (Fink and Smith, 2007). $^{10}$Be/$^{9}$Be ratios were normalised against the NIST - 4325 standard reference material using the revised nominal $^{10}$Be/$^{9}$Be ratio of 2.79 x $10^{-11}$ (Nishiizumi et al., 2007). All isotopic ratios were corrected using full chemistry procedural blanks prepared from purified beryl crystal with a $^{9}$Be concentration of 1120±10 ug/g and giving a measured $^{10}$Be/$^{9}$Be ratio of (4.75 ± 0.11) x $10^{-15}$ (n=7, 3 targets). Background corrections ranged between 2-10% of the measured AMS $^{10}$Be/$^{9}$Be ratios (Table 3). Multiple measurements of individual samples were combined as weighted means with the larger of the mean standard error or total statistical error. Final analytical errors were derived from the quadrature addition of the 1-sigma spread in repeat measure of AMS standards (1.0 – 2.0%), error in the AMS ratio, and a 1% error in Be-spike assay resulting in a combined analytical error ranging from 2.9 to 7.1% for $^{10}$Be/g-quartz excluding 3 samples at ~8.8 to 10.1%. The SUERC samples were processed following procedures outlined for $^{10}$Be in Glasser et al., (2012) and Rolfe et al., (2012). $^{10}$Be/$^{9}$Be ratios were also normalised against the NIST-4325 standard reference material adopting a $^{10}$Be/$^{9}$Be ratio of of 2.79 x $10^{-11}$ (Nishiizumi et al., 2007) (see Table 3) . Between 220 and 250 μg of Be spike was added to samples and procedural blanks. $^{10}$Be blank corrections ranged between 1 and 11% of the measured AMS $^{10}$Be/$^{9}$Be ratio. $^{10}$Be targets were measured by accelerator mass spectrometry at SUERC (Xu et al., 2010).

$^{10}$Be ages were calculated using the Lal/Stone time-dependent scaling scheme (Lm) and the NE North America (NENA) calibration dataset (Balco et al., 2009) with a spallation reference sea level-high latitude production rate of 3.87 ± 0.19 (4.8%) $^{10}$Be atoms/g/a. This value incorporates the re-standardisation of the Nishiizumi standards and half-life revision reported by Nishiizumi et al. (2007). Currently there is no local calibration site for $^{10}$Be production in the High Atlas (31°N); although the NENA calibration dataset is just a little further north (41°N) to Morocco/Iberia on the opposite side of the North Atlantic. In any case, the NENA calibration closely fits the global calibration dataset compilation of Heyman (2014) and ages are within 2% of those calculated using the most recent CRONUS calculator of Marrero et al. (2016).

*3.2.2. $^{36}$Cl Analysis*

Eighteen $^{36}Cl$ samples were prepared for AMS measurement at the SUERC AMS facility. The elemental composition and results of the $^{36}Cl$ AMS analyses are given in Table 4. Elemental analysis of the bulk rock fraction was determined using XRF. Uranium and Thorium concentrations in the bulk rock were determined using ICP-MS. Selected elemental analysis in the processed target fraction (CaO, $K_2O$, $TiO_2$, $Fe_2O_3$) was determined using ICP-OES. Stable Cl concentrations were calculated by AMS isotope dilution (Di Nicola et al. 2009). Standard Z93-0005 with a nominal $^{36}Cl/Cl$ ratio of $1.20 \times 10^{-12}$ (Vogt et al 1994) was used as a primary standard for $^{36}Cl$ measurements. Blank corrections for $^{36}Cl$ concentrations ranged between 0.5 and 25%. All $^{36}Cl$ analyses were performed on the 125-250 μm fraction. For two samples, the processing was repeated commencing from untreated rock powder and using the 125-250 μm mass fraction to asses reproducibility and improve the precision of both Cl and $^{36}Cl$ concentrations (IRHZWE-6 and TAM-5) and for a third sample (AT3a) the larger 250-500 μm fraction was also analysed. The paired ages from two of the replicates (TAM5 and AT3a, Table 4) agreed within 1-sigma uncertainty whilst the third (IRHZWE-6), although deemed to be an outlier, gave very different ages and was rejected. The sample geochemical analyses (from bulk rock and the processed fraction) and AMS results were used to calculate $^{36}Cl$ exposure ages from the CRONUS Earth Web Calculator v.2.0 (Marrero et al., 2016) employing the Lal/Stone time-dependent scaling scheme (Lm). About half of the samples had relatively high levels of stable chloride ranging from ~200 to 522 ppm which can negatively impact $^{36}Cl$ exposure age accuracy because quantifying thermal neutron production of $^{36}Cl$ is a complex problem due to the strong dependency on sample geometry, time dependent uncertainties in neutron moderation and heterogeneity in U-Th distribution (Phillips et al 2012, Schimmelpfennig et al. 2009). Table 5 provides the fractional distribution of total $^{36}Cl$ production from spallation (on Ca and K) and from thermal neutron capture on native $^{35}Cl$ (U-Th radiogenic production of neutrons and neutrons from cosmic ray internations in the rock). All but two of the samples have more than 50% of the $^{36}Cl$ produced from neutron-capture on $^{35}Cl$. According to Phillips et al. (2012), the error in a calculated $^{36}Cl$ age from samples where production is predominantly due to thermal and epithermal neutron capture can be up to 30%, hence in our case, we estimate that for most samples, half the age error stems from high stable Cl content.

Supplementary Table 1 provides the input file for $^{10}Be$ exposure ages via the CRONUS calculator (Balco et al. 2008; 2009).
(http://hess.ess.washington.edu/math/al_be_v22/alt_cal/Balco_NENA_age_input.html).

Supplementary Table 2 provides the input file for the $^{36}$Cl exposure ages via CRONUScalc website calculator (http://cronus.cosmogenicnuclides.rocks/2.0/html/cl/).
Supplementary Table 3 provides the output file for the $^{36}$Cl exposure ages via CRONUScalc website calculator (http://cronus.cosmogenicnuclides.rocks/2.0/html/cl/).

**4. Results: Geomorphology and Geochronology**

Our new mapping, exposure ages and the ensuing discussion are presented with respect to the nine glaciated valleys distributed across three regions or catchments in the High Atlas (Figure 1; Table 1). All $^{10}$Be and $^{36}$Cl exposure ages (quoted with 1-sigma analytical age errors) are summarized in Table 6 and ordered according to our observation of three, spatially distinct and largely temporally separated, glacial units that suggest that at least 3 glacial advances occurred throughout the High Atlas during the last glacial cycle.

Region 1 covers seven major valleys draining the northern and northwestern slopes of Aksoual (3912 m a.s.l.) and Bou Iguenouane (3877 m a.s.l.) peaks (Figure 1 and Figure 3). Five of these valleys drain into the modern river channel of Imenane valley. These valleys, from west to east, are Tamda, Goudmane, Likemt, Iguenouane, and Amguedoul. The remaining two valleys, Tamatert and Imserdane, also drain the same northern slopes, but westward through the villages of Tamatert and Arroumd respectively (Figure 3). The landforms and boulder deposits in Imserdane valley were the focus of a study by Hughes et al (2014), describing the general geomorphology, rock-wall debris, slope failure deposits and glacial geochronology. Samples listed alphabetically in Table 2 from A to U, plus AG and AH, originate from this region. About 2 km due west of Arroumd the second region, Region 2 (Figure 1 and Figure 4) covers Azib Mzik valley draining the northern slopes of Adrar el Hajj (3129 m a.s.l.). Samples listed in Table 2 from V to Z to originate from Region 2. The third region, Region 3, (Figure 1 and Figure 5) covers the greater catchment of Toubkal Massif (4167 m a.s.l.) and the lower northern section of Aït Mizane Valley draining through Arroumd village. This area was mapped for future investigations and six samples (listed as AA to AF) were collected from a valley near the shrine of Sidi Chamarouch. However, moraine successions were not subdivided and ascribed to distinct morphostratigraphical units, unlike those in Regions 1 and 2, because of uncertainties in the relative relations of the various moraines. Further research is needed.

All eight valleys in Regions 1 and 2 contain localised and spatially distinct units of glacially deposited boulder fields or boulder laden ridges, some of which have clearly preserved their moraine shape and orientation with respect to down-valley ice flow. Five of the eight valleys

contain 3 such units. The morpho-stratigraphical succession with respect to elevation and volume of boulders varies between valleys. Five of the valleys contain all three sets of distinct moraine deposits from cirque to maximum extent, usually covering 3-6 km over elevation differences of a few hundred metres. Due to the commonality of this pattern, we have labelled these deposits as Units 1, 2 and 3 with Unit-1 being the most distal (i.e. oldest) (see Table 5). The three remaining valleys, Tamatert, Tamda, Amguedoul, possess only the two oldest units.

The synthesis and glaciological discussion of the overall collection of $^{10}$Be and $^{36}$Cl exposure ages is provided in Section 5.

*4.1 Region 1 - East: Aksoual, Bou Iguenouane and Imenane Valley*

*4.1.1 Description*

The lowest boulder deposits in each of the 5 valleys draining the northern flanks of Aksoual and Bou Iguenouane are found at the banks (predominantly on the southern side) of the Assif n'Imenane River (Figure 3). The river cuts through these boulder deposits near the village of Tacheddirt. These lowest boulder deposits, labelled as Unit-1, are correlated with the lowest elevation deposits in other valleys. The altitude of Unit-1 rises from ~2080 m a.s.l. in the westernmost valley of Irhzer Tamda to 2380 m a.s.l. in the easternmost Amguedoul valley. The boulders have a wide range of volcanic lithologies and include a range of basalt, rhyolite and andesite rock types. Some rest on bedrock with little fine-grain supporting matrix. This is especially true in the lower parts of the Irhzer Likemt Valley where large isolated erratic boulders are perched on bedrock. Matrix-supported boulder-rich diamictons are found exposed in road cut sections in the Irhzer n'Ou Goudmane and Amguedoul Valleys (Figure 6). The sediments in these sections contain a wide variety of volcanic lithologies and clast sizes (from pebble to boulder). In the Irhzer n'Ou Goudmane section the clasts are largely subrounded and subangular (SR: 45%; SA: 35%; A: 20%) and 20% of the clasts are striated. Fine-grained basalts tend to be striated whereas porphyritic volcanic clasts tend not to display striae.

Up-valley of the lowest Unit-1 deposits, a second deposit of boulders, labelled as Unit-2, is present. These are correlated on the basis of morphostratigraphy to Unit-2 in other valleys. Unit-2 has very similar characteristics to Unit-1 being largely subrounded, subangular and containing striated clasts, but differs from Unit-1 in that its moraine morphology is clearer with boulder-rich ridges occurring on either sides of the valleys. In Irhzer Tamda, the Unit-2 ridge of boulders extends to ~2125 m, a short 50 m above Unit-1. In the other valleys Unit-1 and Unit-2 are more widely separated in altitude and distance with the lower limit of Unit-2 increasing to ~2300 m a.s.l. in

Irhzer n'Ou Goudmane, 2500 m a.s.l. in the Irhzer Likemt, 2250 m a.s.l. in the Iguenouane Valley and 2350 m a.s.l. in the Amguedoul Valley.

At elevations closest to headwalls, a third ridge of boulder deposits are found usually in cirque-like positions. These youngest deposits, designated as Unit-3, are valley-correlated and present in only three of the five valleys (Goudmane, Likemt and Iguenouane) at similar lower limit elevations of ~2900 m. As with the lower boulder units, Unit-3 contains clasts of a wide range of volcanic lithologies.

### *4.1.2 Interpretation & exposure ages*

The boulder accumulations in all 5 north trending valleys closely resemble the moraine successions found across the wider Atlas Mountains in regions 2 and 3 (see later). They have morphological and sedimentological properties that are characteristic of moraines consistent with the interpretations of De Martonne (1924) and Celerier and Charton (1923). De Martonne (1924, p. 302) cautioned that some rugged longitudinal ridges in valley floors may be fluvial in origin but noted that ridges on valley sides are likely to be moraines. Differentiating between moraines and high-energy alluvial deposits is most challenging for the lowest, oldest and more degraded moraines. Alluvial fans are sometimes eroded forming enclosing sediment ridges. Thus the criteria for distinguishing these features from moraines include: 1) location relative to fluvial channels and valleys, with perched boulder ridges in wide valleys suggesting a glacial rather than fluvial origin, 2) proximity to higher and younger moraines that are very well-preserved suggesting a recessional sequence (e.g. Figure 3), 3) presence of striated clasts and 4) basic sedimentological properties (e.g., shape, roundness and sorting of clasts). When using these criteria, the glacial deposits in the upper catchments can be clearly differentiated from alluvial fans and fluvial terraces observed in the nearby valleys, such as in the Ourika Valley (Delcaillau et al. 2016) and elsewhere in the High Atlas Mountains (e.g. Mather and Stokes 2017).

Adding to the complexity of interpretation, Dresch (1941, Figure 196, p. 598) identified these deposits as rock glaciers. However, there is no evidence to suggest that these particular features are rock glaciers in the sense of Barsch (1996), i.e. as debris accumulations that move down-valley as a result of permafrost creep. Based on our detailed mapping, we infer that the boulder ridges and deposits in the valleys described above are indeed clearly formed by normal (ice) glaciers. It is possible that at one stage during glacial evolution, that they were debris-covered, but there is no residual morphological evidence to support this. Small rock glaciers are evident in the very highest cirques (Hughes 2018), although these are likely to be recent Holocene features (Vieira et al.,

2017). Dresch (1941) also questioned the presence of moraines in the high cirques, including the highest boulder pile in the Irhzer Tamda (Dresch 1941, p. 599, Figure 197) and instead suggested that these are deposits formed by water torrents. Nevertheless, Dresch (1941, Figure 206) did recognise that small glaciers occupied all the upper headwall areas of many of the valleys. However, the presence of more extensive former valley glaciers recognised by De Martonne (1924, Figure 4, p. 301-302), to have descended as low as 2000 m reaching the thalweg of the Imenane valley, is supported with the evidence presented in this paper.

In Irhzer Tamda valley, a boulder perched on a knoll on the eastern side of the valley associated with Unit-1 yielded a $^{36}$Cl ages of **63.3 ± 5.8. ka** (mean of two replicates at **67.0 ± 4.3 and 59.5 ± 3.9 ka**) (TAM-5 [**F**]). A moraine ridge rising on the valley flanks adjacent to but immediately in-board of the extensive spread of Unit-1 erratics, was assigned as Unit-2. Three boulders at elevations from 2140 to 2240 m gave ages of **29.5 ± 1.7 ka** ($^{36}$Cl; IT-10 [C]) (see Figure 7), **22.5 ± 1.4** and **16.3 ± 0.9** ka ($^{10}$Be; TAM-7 [**D**] and TAM-2 [**E**]). A boulder on the same suite of moraines (Unit-2), and slightly higher in the valley at 2380 m, was at **26.1 ± 1.3 ka** ($^{36}$Cl; TAM-6 [**G**]). A sample from a boulder nearby yielded an outlying age of **6.0 ± 0.4 ka** ($^{36}$Cl; TAM-4).

To the east, in the Irhzer Likemt Valley (Figure 3) at its lowest elevation of ~2300 m, two quartz vein samples from boulders on Unit-1 yielded ages of **13.6 ± 0.9** ka and **34.6 ± 2.0** ($^{10}$Be; Irhzwe-10-11 [**J**] and Irhzwe-9-11 [**H**]). Both boulders are positioned on the crest of the eastern boulder ridge. A sample from the lowest of Unit-2 lateral moraines at ~2400 m in elevation gave an age of **17.2 ± 0.9 ka** ($^{36}$Cl; Irhzwe-12-11 [**K**]). Higher up the valley at ~2575 m, five boulders yielded ages of **8.2 ± 0.5 ka** ($^{10}$Be; Irhzwe-5-10 [**M**]), **8.9 ± 0.6 ka** ($^{36}$Cl; Irhzwe-4 [M]) on the western lateral, and on the eastern lateral, ages **of 25.8 ± 1.6** ($^{10}$Be; Irhzwe-2-10, [L]), **6.3 ± 0.6** ( $^{10}$Be; Irhzwe-7-10 [L]) and **9.0 ± 4.5 ka** (mean of two replicates at 12.2 ± 0.8 and 5.8 ± 0.3 ka) ($^{36}$Cl; Irhzwe-6 [L]). One sample on a boulder-filled extension of the western lateral, just below the cirque moraine, gave an age of **16.6 ± 0.8 ka** ($^{36}$Cl; Irhzwe-3 [**N**]). The highest moraines in the Irhzer n'Likemt, labelled as Unit-3 in Figure 3, is located just below headwall and form prominent arcuate boulder piles at the lip of a deep cirque on the northern cliffs of the Tizi Likemt at 3555 m (Figure 8). Two samples yielded exposure ages of **12.1 ± 0.8 and 13.7 ± 0.8 ka** ($^{10}$Be; Irhzwe-1 [P] and Irhzwe-8-10 [**Q**]). There are clearly several young outliers in Units-1 and -2 in Irhzer Likemt, which are likely to be the result of exhumation caused by erosion of the moraines.

Five samples from Unit-1 moraines in the Amguedoul Valley, the most easterly of the glaciated Imenane Valley tributaries, yielded ages of **12.6 ± 0.8, 87.9 ± 4.7, 9.1 ±0.5 ka** and **9.5 ± 0.7 ka**

($^{10}$Be; Amguedoul-7,- 2,- 3 and -6, respectively [**R, S, T, U** in Figure 3] and **80.0 ± 12.1 ka (**$^{36}$Cl; Amguedoul-1, [R]) (Figure 9). Whilst all of these samples are from moraine crests, these sites are prone to torrential erosion by nearby streams and slope processes, especially the area around samples T and U (Figure 3), and again, the youngest ages are likely to be the result of exhumation caused by erosion of the moraines. This interpretation is compounded by the fact that moraines are the lowest of the valley and would be expected to be the oldest too (see Figure 3). The fact that the two oldest boulder ages are very similar yet from different boulders on the same moraine crest suggests that the ages are 'real' exposure ages and not inherited. Furthermore, the similarity of the $^{10}$Be and $^{36}$Cl ages provides confidence in the age calculations.

### *4.2 Region 1 West: Aksoual and Assif Tamatert*

#### *4.2.1 Description*

Unit-1 boulders are found in the valley immediately above the village of Tamatert at 1900-2000 m a.s.l. Here, several large subrounded basalt, diorite and rhyolite boulders are perched on the valley side as well as close to the modern river channel. The largest of these are >10 m in diameter and a 12-m diameter basalt boulder on the western side of the valley overlies a diamicton containing erratic diorite clasts. Whilst the bedrock is basalt in this area, the diorite originates from higher in the catchment. A truncated basalt spur occurs on the western side of the lower Assif n'Tamatert at 2000 m a.s.l. (Figure 10) with large subrounded boulders perched on the up-valley side of the spur. At 2100-2200 m a.s.l. a dense accumulation of igneous erratic boulders, originating from the cliffs higher in the valley, forms a boulder ridge on a bedrock spur. This boulder ridge runs from the modern river channel up a bedrock spur with the highest boulders situated ~100 m above the channel. The boulders (sample n = 20) are dominated by subrounded, subangular and angular shapes (A: 30%; SA: 35%; SR: 35%) and several boulders are striated (n = 5). All of the boulders of the lower Assif n'Tamatert are correlated with the Unit-1 deposits in other valleys. A second concentration of boulders on both sides of the valley is present 300 m up-valley at 2300-2400 m.

#### 4.2.2 Interpretation & exposure ages

The two boulder units described above are correlated with Unit -1 and -2 moraines in other valleys. The steep nature of this valley suggests that moraine preservation, particularly in the steepest and narrowest sections, would have been limited and explains the sparse distribution of boulders and absence of distinguishable or contiguous moraine in Assif n'Tamatert. Nevertheless, the truncated spur overlaid with perched boulders provides support for interpretations of an ice limit as low as 1950 m a.s.l. in this valley. The moraines of Unit-1 between 2100 and 2200 m a.s.l. are the best-preserved moraines in this valley and are situated in an area where the valley broadens out.

Samples from two large erratic boulders on the moraine crest yielded exposure ages of **60.0 ± 4.7 ka** ($^{36}$Cl; AT-4 [**A]**) and **40.5 ± 3.5 and 38.5 ± 3.5 ka** (mean age = **39.5 ± 5.0 ka**) from a duplicate sample ($^{36}$Cl; AT-3a [**B**]).

*4.3. Region 1 (west): Aksoual and Assif n' Imserdane*

The Assif n'Imserdane is an eastern tributary of the lower Aït Mizane valley and is situated below the 1500-m high cliffs of Azrou n'Tamadôt (3770 m a.s.l.) which represents the western ridge of Aksoual (3912 m a.s.l.). The valley is dominated by rock avalanche deposits that yielded an average exposure age of 4.5 ± 0.5 ka (landslide units A and B in Hughes et al., 2014, Table 2). Moraines also occur in this valley, an observation made by De Martonne (1924), and several striated boulders are present (Figure 6). Similarly as seen in the adjacent valleys, three separate moraine units occur, closely spaced in both distance and altitude compared with the Toubkal Aït Mizane Valley of Region 3; see below) with moraines at 1900-2300, 2150-2350 and 2350-2400 m a.s.l. (Figure 3) and again these correlate to Units -1, -2 and -3. Two exposure ages from Unit-2 of **4.4 ± 0.9 ka** ($^{36}$Cl; A-12 [**AG**]) and **1.1 ± 0.2 ka** ($^{36}$Cl; A-14 [**AH**]) now supplement a previously published set of eight $^{10}$Be exposure ages (Hughes et al 2014) from Units 1 and 3 which ranged from 1.5 to 7.5 ka (total mean of 4.2 ± 2.0 ka). With the addition of the two new $^{36}$Cl ages, all of the 10 ages from moraine Units -1, -2 and -3 in the Assif n'Imserdane are similar to the adjacent rock avalanches confirming Hughes et al. (2014) conclusion that the surfaces of these moraines deposited during the late Pleistocene had been significantly altered at the time of major rock avalanche(s) at ~4.5 ka. The youngest ages i.e. ([AF] and A32-11 in Hughes et al 2014) may be related to erosion caused by grazing as has been shown for the last 1.5 ka in this same valley by Fletcher and Hughes (2017). The interpretation presented by Hughes et al. (2014) that the Imserdane landforms are the result of slope failure or rock avalanche means that their earlier interpretation as rock glaciers (e.g. Dresch 1941; Mensching, 1953; Chardon and Riser, 1981) were incorrect. The exposure ages illustrate the degree of landform modification with none of the 10 boulders sampled on moraine surfaces in the Assif n'Imserdane valley yielding an original Pleistocene age.

*4.4 .Region-II : Adrar el Hajj and Azib Mzik valley*

*4.4.1 Description*

The Azib Mzik valley is situated 1000 m below the north-facing cliffs of Adrar el Hajj (3129 m a.s.l.) about 2-3 km immediately to the west of the villages of Imlil and Arroumd (Figure 4). A series of sediment-boulder ridges closely spaced in both distance and altitude are present within this short valley, the lowest of which is at ~1950-2100 m a.s.l. on the north side of the valley. The

boulders are large (up to 10 m in diameter) and predominantly subrounded (50%) and subangular (40%) with a small proportion angular (10%) and have a wide variety of igneous lithologies including a variety of grades of basalt, andesite, rhyolite. These igneous boulders are erratics and rest on Triassic sandstone basement on the northern side of the valley. On the south eastern side of the valley, igneous erratics are perched on a rocky rhyolite bedrock promontory which guards the entrance to Azib Mzik at 2050-2100 m. The lowest boulder accumulations in the Azib Mzik valley define Unit-1 (Figure 4). At about 200 m distance up-valley of Unit-1, a second set of sediment-boulder ridges (Unit-2) are present forming a distinct linear sediment ridge oriented NE to SW and which extends over an elevation of 2050-2400 m. The ridge underlying the boulders is exposed by the stream on the north side and appears as a matrix-supported diamicton with a wide range of igneous clast lithologies (basalt, andesite, rhyolite). Unit-2, dissected by the modern stream, continues on the eastern flank. The surface boulders are dominated by subangular and subrounded shapes (VA: 5%; A: 15%; SA: 40%; SR: 40%). The next up-valley boulder rich ridge formation, Unit-3, is similar in morphology and lithology to Unit-2 but is distinctly nested within Unit-2. Both lateral ridges of Unit-3 extend ~250 m in elevation and its lowest point is ~100 m above Unit-2 where the modern stream dissects it.

4.4.2 Interpretation & exposure ages

The series of sediment-boulder ridges in the Azib Mzik valley have the attributes of moraines. The boulders are a mix of igneous erratics that have been transported from the backwall cliffs of Adrar el Hajj which arc around the south of the valley forming a shallow cirque (Figure 4). The fact that many of the boulders are subrounded and subangular supports subglacial abrasion. Other more angular erratics are likely to have had a supraglacial path. The moraine surfaces yield markedly different ages and become successively younger towards the backwall at the northern cliffs of Adrar el Hajj. A boulder in the lowermost Unit-1 moraines gave an age of **7.2 ± 0.6 ka** ($^{36}$Cl; AM11-11 [**V**]). This boulder was on a moraine ridge situated on a steep slope close to the main river channel and the moraine is likely to have been eroded, explaining its young age. In contrast, two perched erratics in a stable position on the rock promontory on the east side of the valley yielded exposure ages of **44.2 ± 2.6 and 33.4 ± 1.9 ka** ($^{10}$Be ; AM-2, AM-3 [**W**]). Quartz veins from boulders on Unit-2 moraine crests in the middle of the valley yielded $^{10}$Be exposure ages of **18.6 ± 1.0 and 25.3 ± 1.4 ka** (AM-10-11, AM-7, [X]) whilst an adjacent andesite $^{36}$Cl sample gave an age of **2.7 ± 0.9 ka** (AM-8-11, [X]). Samples from two boulders, on the western lateral moraine of Unit-3 yielded a $^{10}$Be age of **11.5 ± 0.7** (IGL-7) and a $^{36}$Cl age of **13.2 ± 0.7 ka** (AM-9-11) (both labelled as Y in Figure 4). Two more samples associated with this moraine unit gave $^{10}$Be ages of **12.5 ± 0.8 ka** (IGL-10, and **11.5 ± 0.7 ka** (AM-4) (both labelled as Z in Figure 4).

IGL-10 was from a large boulder on the opposite eastern moraine crest whilst AM-4 was sampled from a large bedrock outcrop exposed in a meltwater channel in the valley below these moraines (Figure 4).

*4.4. Region 3: Toubkal – Assif n'Aït Mizane*

The Aït Mizane Valley stretches 12 km from the summit of Toubkal (4167 m a.s.l.) to the village of Imlil (1750 m a.s.l.) (see Figs 1 and 5). Here we focus on the lowest glacial features in the Aït Mizane Valley, which represents the upper section of the Rheraia Valley containing Assif n' Aït Mizane and separates Adrar el Hajj from Aksoual. The Aït Mizane Valley is much longer than the Mzik Valley and the glacial landforms in the former are spread out by much larger distances (9 km; see Table 1). The style of glaciation in this area was very different with ice-field and outlet glaciers compared to the valleys of Adrar el Hajj and Aksoual/Bou Iguenouane that exhibit typical valley glaciers. The central Toubkal area is the focus of continuing research and our current geomorphological mapping across the valley area is provided in Figure 5.

*4.4.1 Description*

At the village of Arroumd, the Aït Mizane Valley is blocked by a distinct pile of rocks that emanates from the Assif n'Imserdane below the northwest face of Aksoual (see Section 4.3 above). Beyond this constriction is a large area of gently sloping gravels forming a braidplain occupied by ephemeral streams that extends for about 1 km. At the up-valley end of this braidplain at an elevation of ~1850 m, the valley narrows and on the western flank of the main river channel is filled by a large mound of boulders. The distal profile of this mound is ~40 m high and steeply inclined. Sections through the mound reveal a matrix-supported diamicton. The clasts vary in size from cobble to boulder. The clasts (n=50) are largely subrounded and subangular (VA: 10%; A: 20%; SA: 30%; SR: 30%; R: 10%), and 20% are striated (see Figure 6). They have a strong clast fabric dipping up-valley and cover a range of igneous lithologies including basalt, andesite, rhyolite, granites and also conglomerates. Many of these are erratic to the underlying basalt bedrock in this area. On the surface of the mound the mean height of the 10 largest boulders is 12.6 m. On the western side of the main river channel a line of similar boulders can be traced 200 to 300 m up-valley. These boulders start at the river channel near the opposite boulder mound described earlier and trend upslope reaching a position 50-100 m above the river channel. Up-valley interlocking spurs have been truncated and bedrock appears moulded and is striated in several places. Boulders are often perched on bedrock obstacles well above the narrow gorge occupied by the modern river channel.

4.4.2 Interpretation and correlations

The matrix supported boulder mounds, boulder accumulations and bedrock ridges described above are all considered to be glacial in origin and are interpreted as moraines associated with different advances and also standstills at 'pinch-points' within the valleys. Whilst at least three morphological units can be identified based on position in the landscape, the stratigraphical correlations with other valleys remains uncertain. This is because of the much larger and longer cirque-valley systems draining into the Mizane Valley and also the lack of dating, especially on the higher moraines. Stratigraphical units are therefore not indicated in Figure 5.

The lowermost moraine is close in altitude to the lowest moraine in the Mzik Valley. These moraines have been overlooked in previous research which places the lower limit of glaciation in the Toubkal region at 2600 m a.s.l. (Heybrock 1956; Messerli 1967; Chardon and Riser 1981; Messerli and Winiger 1998), at elevations where moraines are morphologically very clear. Despite the lower moraines not having the morphological clarity of higher moraines, they are still prominent features in the valley, contain erratic boulders much larger than could have been transported by rivers and are located far above and distant from the drainage channel. This, combined with sedimentological data exposed in sections, the presence of numerous striated erratic clasts, and erosional evidence of the truncated spurs below Sidi Chamarouch (Figure 10), provides clear and irrefutable evidence of glaciation down to just below 2000 m a.s.l. Around Sidi Chamarouch the large concentration of moraines represents an important 'pinch-point' for glacier dynamics in this valley where it enters a steep-sided gorge. Roche moutonées, perched boulders and moraines in the Tizi n'Tarharate valley provide information on the glacier succession into some of the highest parts of these mountains, in this case directly below the northwestern face of Adrar n'Tichki (3753 m a.s.l.).

Six ages were obtained from the lowest valley section, four from the boulder mounds just upstream of the braided fluvial gravel deposits where the valley narrows and two at higher elevations on moraine ridge crests associated with younger advances. A large boulder from the lowermost moraine yielded a $^{36}$Cl age of **50.0 ± 4.9 ka** (TOUBKAL-4 [**AA**]) (Figure 11). Just 200 m distance up-valley, a basalt boulder precariously perched on a bedrock promontory, ~75 m above the river on the eastern side of the valley, gave a $^{36}$Cl age of **28.9 ± 1.4 ka** (TOUBKAL-3 [**AB**]). A further 750 m up-valley, a quartz-vein striated bedrock on the eastern edge of the ravine gave a $^{10}$Be exposure age of **28.2 ± 1.5 ka** (TOUBKAL-2 [**AC** ]). However, this site was located right on the gorge edge and was strongly shielded by a rock promontory just 1 m away immediately to the NE. A second bedrock quartz vein sample from glacially polished bedrock, just 25 m distance to the

south, yielded a $^{10}$Be exposure age of **52.0 ± 3.1 ka** (TOUBKAL-1 [**AD**]). Both of these sites are opposite a clear truncated spur on the opposite side of the valley. Samples TOUBKAL-4 and -1 (the older ages) are from the largest boulder and bedrock and likely to be the more stable and reliable sites. The fact that TOUBKAL-4 is from a boulder also negates the probability of inheritance in TOUBKAL-1, the bedrock sample.

In the Unit 2 moraines around Sidi Chamarouch a large (c. 1 m high) quartz boulder above the settlement on the northern side of the valley gave a $^{10}$Be exposure age of **7.1 ± 0.4 ka** (SC-1 [**AF**]). This boulder can be traced to a quartz band on the cliffs of Aguelzim visible to the southwest, although the boulder must have been dragged to the northeast and not simply rolled. The young age suggests exhumation. No other boulders were dated from the moraine concentration around Sidi Chamarouch. Across the valley, perched above Sidi Chamarouch, a quartz sample from a striated roche mountonee on the rock step guarding Tizi n'Tarharate gave a $^{10}$Be exposure age of **11.7 ± 0.7 ka** (TT-1 [**AE**]). This is a stable and reliable site where exhumation and inheritance are unlikely. This surface is therefore more likely to be associated with Unit 3 surfaces dated elsewhere and as such is grouped with these in Table 6. However, as noted earlier, further work is needed to clarify the glacial stratigraphical sequence in Region 3.

*4.5 Comparisons with other parts of Toubkal*

There is evidence for extensive glaciation in the mountains neighbouring the study areas presented in this paper, namely around the peaks of Annrhemer (3942 m a.s.l.) Adrar n'Dern (4001 m a.s.l.), Ouanoukrim (4089 m a.s.l.), Tazaghart (3980 m a.s.l.) and on also the southern and eastern sections of Toubkal (4167 m a.s.l.) (see Figure 1). West of Ouanoukrim some of the most extensive ice masses of the Atlas occurred, with evidence for plateau ice fields forming over the Tazaghart plateau with numerous outlet glaciers descending 5-10 km towards Tisgui and also further north into the Azzaden valley, reaching altitudes of < 2000 m a.s.l. (Figure 1) (Hannah et al., 2016). There is also evidence for more than 3 glacial units in these highest parts of Toubkal massif with Hughes (2014) and Hannah et al. (2016) recognising a 4$^{th}$ moraine unit below the northern cliffs of Tazaghart and suggested that these deposits may be Holocene, possibly Little Ice Age, since a permanent snow field exists immediately up-valley from this moraine today (Hughes 2014). It is possible that a 4$^{th}$ glacial unit representing Holocene glaciers is present also in other areas, especially in the highest cirques. Large glaciers also formed in the cirques and valleys directly to the east of Toubkal summit with ice possibly descending 6-7 km to as low as 2100 m at Tissaldaï.

Further east large glaciers formed in the valleys around Adrar n'Dern. The fronts of these glaciers reached the Assif n'Tinzer near the village of Azib Likemt (Figure 1). However, as with the eastern areas of Toubkal, further research is needed in this area to confirm the exact limits of the former glaciers in the Adrar n'Dern area.

Finally, there is also clear evidence of glaciation in the cirques and valleys of Annrhemer (3942 m a.s.l.) and Angour (3614 m a.s.l.) to the north east of Aksoual. In the Angour area, glaciers reached down to the ski station near Oukaimeden and several generations of moraines have been identified. These areas within the greater High Atlas Mountain ranges will be the focus of future research studies which will require further mapping and careful sampling for exposure ages to consolidate the regional glaciology and confirm the exact limits and timing of former glaciers in the High Atlas.

## 5. Discussion

### *5.1 Glacial sequence and age correlations*

The glacial sequence in the High Atlas Mountains of Morocco shows that the last glacial cycle is represented by a series of moraines with exposure ages ranging from 88 to 10 ka. When obvious outliers, i.e. those samples whose ages are inconsistent with respect to elevation and average age of residual samples, are removed, then the exposure ages reveal a pattern of successively diminishing glacier extent in each valley through the last glacial cycle. Three discrete moraine accumulations can be recognised in the valleys of the Toubkal massif and these correspond to three separate phases of glaciation with a combined average $^{10}$Be and $^{36}$Cl exposure age for the oldest of 50.2 ± 19.5 ka (1 SD, n= 12, 7 outliers) , then a phase commensurate with the global LGM period of 22.0 ± 4.9 ka (1 SD, n=9, 7 outliers) and the youngest and highest in elevation 12.3 ± 0.9 (1SD, n=7 no outliers) that falls in the Younger Dryas chronozone (Figure 12).

The lowest elevation moraines are associated with the oldest and most extensive glaciation (Unit-1) and yield a wide scatter of 12 ages between 88 (Amguedoul-2) and 28 ka (Toubkal-2 and -3), with 7 outlier ages all being younger and between 13.6 ka to 6.0 ka. These outliers are unlikely to represent glacial ages (especially the numerous Holocene ages) and instead are likely to be explained by boulder exhumation as moraines were eroded. These lowest moraine surfaces clearly pre-date the global LGM. The mean age (excluding younger outliers) is 50.2 ± 19.5 ka (Table 6) and the large 40% spread, together with a far younger outlier population, clearly indicates that surface modification and other geological processes are active leading to apparent exposure ages

that are too young. Under this scenario, if we assume that inheritance is not a relevant process, then the two oldest ages are more representative of emplacement and thus indicate a maximum advance at 80-90 ka (MIS 5b). Whilst this coincides with a humid phase in North Africa, it also coincides with a peak in solar radiation at 30°N and warm sea surface temperatures in the North Atlantic (Figure 12). Thus, this age for the maximum glacial advance seems improbable. There are no clear age clusters younger than this maximum although 8 of the 12 ages range from 63 ka to 35 ka, with the remaining two at 28 ka, which may indicate a series of successively smaller glacier advances or standstills through MIS 4 and 3. However, the morphostratigraphical evidence for this is not obvious since all 12 ages originate from Unit-1 moraines that are designated as time-equivalent. It is also possible that this oldest glaciation occurred during the Middle Pleistocene and that all 12 exposure ages simply reflect a complex exhumation and erosion history in this active tectonic landscape through the Middle and Late Pleistocene. In the Ourika Valley, which is just a few kilometres northeast of the study area (see Figure 1), Delcaillau et al. (2016) argued that intense rainfall events during the Middle Pleistocene resulted in increased erosion and transport of sediment from the hillslopes into the trunk river. However, this sediment delivery could equally be associated with meltwater discharge from Middle Pleistocene glaciers in the upper catchment of the Ourika Valley, including the extensively glaciated upper catchment around Angour (3616 m a.s.l.) and Annrhemer (3942 m a.s.l.) as well as up-valley of the Kissaria Gorge on the northern slopes of Adrar n'Dern (4001 m a.s.l.) (Figure 1). Middle Pleistocene glaciations were the most extensive glaciations in the Pyrenees (Calvet et al., 2011), the Italian Apennines (Giraudi et al. 2011) and the Balkans (e.g. Woodward et al. 2004; Hughes et al. 2006, 2011b; Woodward and Hughes 2011). Nevertheless, if we take the oldest moraine ages at face value then the chronology is not implausible since in many Mediterranean mountains, there is evidence that the most extensive glacier advance of the last glacial cycle pre-dates the global LGM (Hughes and Woodward 2016). An early, pre-LGM, glacier maximum during the last glacial cycle has been reported from the Cantabrian Mountains, Spain (Serrano et al. 2016), the Pyrenees, France/Spain (Pallas et al. 2010) and Greece (Pope et al. 2016). Indeed, this situation is observed on many mid-latitude mountains around the world (Gillespie and Molnar 1995; Hughes and Woodward 2008; Hughes et al. 2013)

A second set of moraine surfaces (Unit-2) can be identified having a more clustered age range between 30 (IT-10) and 17 (TAM-2 and Irhwze-3) ka, with 7 outliers all being younger and between 9 and 1 ka – a similar outlier age range as seen for Unit-1. Nine exposure ages have a mean age that overlaps with the global LGM (cf. Hughes and Gibbard 2015; 27.4-23.3 ka). Their mean age (excluding younger outliers) is 22.0 ka ± 4.9 ka (Table 6).

The third and final moraine landform, at the highest elevations is the youngest and yielded exposure ages of 13.7 ± 0.8 to 11.4 ± 0.7 ka (n = 7) with a mean age of 12.3 ± 0.9 and no outlier ages (Table 6). All of these ages overlap with the Younger Dryas (12.9-11.7 ka).

Whilst three distinct moraine units are identifiable in the morphostratigraphical record (Units 1 to 3) the age scatter becomes greater with increasing moraine age, i.e. the greatest scatter on the oldest Unit 1 moraines and the least scatter on the youngest Unit 3 moraines (Table 6). This is illustrated by the standard deviations for the ages from each unit which simply reflect the decreasing probability of preservation for the older deposits compared with younger surfaces, as observed in numerous studies where cosmogenic exposure ages are associated with pre-LGM glacial events (Heyman 2014). The excessively large scatter in the older moraine units may also be because these lower moraines may represent a series of standstill or retreat moraines, i.e. the surfaces of moraines such as Unit 1 represent diachronous surfaces. This is explored further below.

At Arroumd, Chardon and Riser (1981) suggested that three generations of glaciation and rock glacier activity were evident, during the early Würmian at 45 ka, between 20 and 15 ka and during the Late-glacial (13-10 ka). When the hypothetical three-phase chronology suggested by Chardon and Riser (1981) is applied to other valley glaciers mapped and dated in the region, it is remarkably close to the cosmogenic exposure age chronologies However, ironically, moraines in the Arroumd valley have been shown to be strongly disturbed by catastrophic rock slope failures and rock glaciers re-interpreted as rock avalanche deposits. So whilst Chardon and Riser (1981) were correct in their hypothetical glacial-age sequence their geomorphological interpretations has now been revised (Hughes et al. 2014).

*5.2 Moraine erosion and ages*

As already noted, apart from the youngest glacial phase, Unit-3, there is significant scatter in ages from the two older Pleistocene Unit-1 and Unit-2 moraines (see Table 6). We consider 14 of the 42 samples to be outliers and these are excluded from the summary statistics in Table 6. This is because they are clearly inconsistent with the morphostratigraphical sequence, are all more than half the mean age of their associated glacial Unit and 12 of the 14 are Holocene in age. Taken as a complete group, the mean outlier age is 7.6 ± 3.4 ka (n=14). However, if any cluster exists within the outlier set, the most discernible is that the ten mid to early Holocene samples have the same mean but half the spread, i.e. 7.6 ± 1.7 ka (n=10). This cluster of 10 of the 14 outliers sits comfortably within the early Holocene (~10 to 5 ka), when the neighbouring Sahara Desert

supported widespread vegetation and lakes during the interglacial phase of the African Humid Period (de Menocal 2008). If moraine disturbance and/or exhumation occurred at a steady rate through time then more very young (<5 ka) samples across the late Holocene would be expected. However, after 5 ka climate was much drier in North Africa (de Menocal 2008; Tjallinghii et al. 2008) and the majority of the exposure age evidence suggests deep erosion of moraine surfaces was not significant. This is despite clear evidence of the Late Holocene soil erosion in this area linked to human occupation and associated grazing (Fletcher and Hughes 2017) and the inherent susceptibility of soils to high-magnitude rainfall erosion events in semi-arid environments. Earlier humid periods in the last glacial cycle were never as wet as in the Early Holocene (Figure 12) although it cannot be discounted that earlier humid periods were associated with moraine disturbance, especially for the oldest moraines.

Seismic activity may also explain localised moraine disturbance in some valleys. Whilst there is evidence to suggest that High Atlas has been relatively tectonically quiescent, especially for the Middle-Late Pleistocene (Stokes et al. 2017), localised seismicity in the vicinity of major faults remains a significant factor in landscape stability even today (El Alami et al. 2004). For example, in the Arroumd valley, all the moraine exposure ages are Holocene and correspond closely with the exposure ages of rock avalanche deposits in this valley (5-4 ka) (Hughes et al. 2014). These ages are not replicated in any other valleys and this indicates that surface disturbance associated with seismic activity can be very localised. This has significant implications for sampling for cosmogenic exposure dating and suggests that in tectonically-active areas more than one valley should be sampled in order to fully assess glacial chronologies. In the Imenane valley, moraines display evidence of neotectonics with faulted moraines in several locations. It is possible that the young outliers (which were all from the Imenane valley) are associated with seismic activity along the faults associated with Tizi n'Test fault complex which run through these moraines. However, further evidence is needed to date fault movements within Quaternary deposits in this valley. At the present time we can only speculate as to the causes of clustering of Holocene outlier ages on the Pleistocene moraines, although their significance for understanding landscape evolution should not be dismissed.

In summary, it is evident from this dataset that it is extremely difficult to obtain precise moraine chronologies for moraines older than 20-30 ka in an active tectonic landscape like the High Atlas. Despite these difficulties, this is an area that lacks any previous knowledge of geomorphological history and the timing of major landscape events. Thus, the new data presented here is a major contribution to beginning to understand the timing of glaciations in this region.

*5.3 Climatic significance of the High Atlas glacial record*

The new High Atlas glacier sequence correlates clearly with more northerly areas of the NE Atlantic where a pre-LGM glacier maximum is frequently recorded (e.g. Pallas et al. 2010; Serrano et al. 2016; Rolfe et al. 2012). The global LGM in the NE Atlantic is also recorded by a significant glacier advance in both the British Isles (Clark et al. 2012) and Spain (Palacios et al. 2011). The global LGM is also recorded in moraine sequences in the easternmost mountains of the Mediterranean (Akçar et al. 2016) and whilst sometimes smaller than earlier Late Pleistocene advances (e.g. Pope et al. 2016), glaciers during the global LGM are clearly recorded across the Mediterranean mountains. The Younger Dryas is clearly recorded in mountains all the way along a transect from Morocco (this paper), Spain (Palacios et al., 2012), the British Isles (Ballantyne 2007; Hughes 2009) and Norway (Lohne et al., 2012). This is to be expected given the role of the North Atlantic Ocean in forcing this climatic perturbation (Bakke et al., 2009). In the eastern Mediterranean the Younger Dryas is also recorded by cirque moraines (Çiner et al. 2015; Pope et al. 2016; Gromig et al. 2017) and this highlights the influence of the North Atlantic Ocean in driving glacier oscillations across the Mediterranean mountains.

Figure 12 shows the timing of the High Atlas glaciations based on our moraine ages in context alongside North Atlantic sea surface temperatures (Bard 2002) and an African Humidity index (Tjallinghii et al. 2008) for the last glacial cycle. The oldest phase (unit-1) of 50.2 ± 19.5 ka ages span MIS 4/3, and covers an interval that was characterised by a relatively wet phase, which would have been favourable for glacier expansion, more so during 45-60 ka . However, we remain cautious with this association given that our broad age range for Unit-1 shown in Figure 12 clearly reflects the impact of geomorphic processes that have modified the true moraine deposition age. . As we noted earlier, given our assessment that boulder exhumation is evident, it is reasonable to conclude that Unit-1 glaciation may overlap with the increase in humidity seen between c. 75 to 88 ka associated with increased summer insolation (Figure 12). Although difficulty in providing a robust climatic interpretation for the oldest moraines is not surprising given the excessive scatter, the ages from younger moraines provide much stronger certainty as to their age. The younger Unit-2 and Unit-1 moraines show a clear correlation to the global LGM and the Younger Dryas. The latter moraines dating to 22.0 ± 4.9 ka correspond with a period of cold sea surface temperatures in the North Atlantic and an insolation minima (Figure 12). Though conditions would have been dry prior to the onset of MIS 2, the increasing humidity early in MIS-2 may have favoured glacier expansion at a time of low insolation (Figure 12). The youngest moraines date to12.3 ± 0.9 which

sits within the Younger Dryas (12.9-11.7 ka). In contrast to the global LGM, this interval was characterised by a peak in insolation. However, a trend towards greater humidity started at c. 15 ka marking the onset of the Africa Humidity Period marked by dramatic increase in vegetation in the Sahara region (de Menocal 2008; Tjallinghii et al. 2008, their Fig. 3). Thus, it is likely that Younger Dryas glaciers were driven by wetter conditions than glaciers during the global LGM. As noted above, the next step is to model the glacier-climate conditions in the High Atlas at these times. With the new glacial chronology of the High Atlas now available, glacier equilibrium line altitudes can be reconstructed at known points in time to provide climatic constraints during the last glacial cycle for the paleoclimate modelling community. This will now be a priority and the focus of future work.

The timing of glaciation in Morocco has major implications for downstream fluvial processes and wider landscape change during Pleistocene cold stages, as has been noted in other glaciated Mediterranean mountain areas (Lewis 1992; Woodward et al. 1992, 2008; Adamson et al. 2014). On the piedmonts of the High Atlas large alluvial fans are present and in the Marrakech area these were fed by rivers draining the glaciated upper catchments of the High Atlas (see Delcaillau et al. 2010). On the south side of the High Atlas, in the Ouazarzate Basin, large-alluvial fans are also present and appear to be largely tectonically-controlled (Stokes et al. 2008). However, there is evidence of significant climate forcing with fan morphologies explained by the interplay between catchment geology, morphology, climate, and flood regime (Stokes and Mather 2015). These fan surfaces have been dated, using $^{10}$Be, to the Middle and Late Pleistocene (Arboleya et al., 2008) and the sediments dated using OSL (Stokes et al., 2017). The $^{10}$Be chronologies from Arboleya et al. (2008) in the Tagragra and Madri River areas included a major fan surface interpreted by the authors as indicating major fan aggradation during MIS 5e (84-121 ka); although, these exposure ages will now be older since they were calculated using a production rate value of 4.98 atoms g$^{-1}$. However, significantly, a major phase of aggradation is identified in fan sediment records in the Dades Gorge area, east of the area studied by Arboleya et al. (2008), dating to c. 74 ka (from quartz) and 92 ka (from feldspar) is identified in Stokes et al. (2017). These ages coincide with the oldest ages from the lowest moraines on the northern side of the High Atlas. There are still uncertainties surrounding the extent of glaciations in the upper catchments feeding these rivers. In the eastern High Atlas glaciation appears to have been strongly focused on the northern slopes with little reported evidence on the southern flanks, such as around the M'Goun massif (e.g. Wiche 1953; Hughes et al. 2004). Future work is needed to target the river valleys known to drain the largest glaciers of the High Atlas; especially those draining towards the Marrakech piedmont where major river terraces and alluvial fans are present.

## 6. Conclusions

The Marrakech High Atlas, Morocco, was extensively glaciated during the Pleistocene. Ice fields and valley glaciers formed during the most extensive glaciation producing moraines as low as 2000 m a.s.l. This paper presents field evidence from the northern flank of this massif in cirques and valleys draining the peaks of Adrar el Hajj (3129 m a.s.l.), Aksoual (3912 m a.s.l.) and Bou Iguenouane (3892 m a.s.l.) as well as Toubkal (4167 m a.s.l.), the highest peak in North Africa. Three discrete moraine accumulations exist in each valley and these correspond to three separate phases of glacier advance or sustained stabilisation with average ages of c. 50 ka, 22 ka and 12 ka. This geochronology is most secure for the younger two moraine units and clearly identifies the presence of a global LGM and Younger Dryas glacial signal in the High Atlas. The older moraine unit is consistent with an early glacier maximum in the Late Pleistocene pre-dating the global LGM. However, the landscape instability inherent with a very active uplifting massif like the High Atlas means that dating moraine surfaces this old remains problematic.

## Acknowledgements

We would like to thank two anonymous reviewers for their comments on this paper and helpful suggestions for improvements. This research was funded by a Thesiger-Oman International Fellowship (2008) and Fieldcentre Grant (2013), both awarded by the Royal Geographical Society (with Institute of British Geographers). Funding was also received from the British Society for Geomorphology, the Quaternary Research Association and The University of Manchester. $^{10}$Be analyses at SUERC were funded by the UK Natural Environment Research Council (Cosmogenic Isotope Analysis Allocation # 9038.1007 & 9070.1009). We would also like to thank Christoph Schnabel formerly at the NERC Cosmogenic isotope Analysis Facility at SUERC, for help in the initial stages of this project and Chalreas Mifsud for sample prepartion at ANSTO. Jamie Woodward, Peter Ryan, John Nudds, Jeff Blackford and several generations of students at the University of Manchester helped with the fieldwork over the past decade. AMS measurements at SUERC were carried out by Sheng Xu. We would like to thank Graham Bowden (University of Manchester) for producing all of the figures. Finally, we would like to thank staff at Dar Imlil, the Kasbah du Toubkal and Gîte Tamatert and our many friends in the Imlil area for their help in undertaking this research.

## References

Akçar, N., Yavuz, V., Ivy-Ochs, S., Reber, R., Kubik, P. W., Zahno, C. & Schlüchter, C. 2014. Glacier response to the change in atmospheric circulation in the eastern Mediterranean during the last glacial maximum. Quaternary Geochronology, 19, 27-41.

Akçar, N., Yavuz, V., Yeşilyert, Ivy-Ochs, S., Reber, R., Bayrakdar, C., Kubik, P. W., Zahno, C., Schlinnegger, F., Schlüchter, C. 2016. A synchronous Last Glacial Maximum across the Anatolian peninsula. In: Hughes, P. D. & Woodward, J. C. (ed.) Quaternary Glaciation in the Mediterranean Mountains. Geological Society, London, Special Publications, 433. http://doi.org/10.1144/SP433.7

Adamson, K.R., Woodward, J.C., Hughes, P.D., 2014. Glaciers and rivers: Pleistocene uncoupling in a Mediterranean mountain karst. Quaternary Science Reviews 94, 28-43.

Andersen, K.K., Svensson, A., Johnsen, S.J., Rasmussen, S.O., Bigler, M., Röthlisberger, R., Ruth, U., Siggard-Andersen, M.-L., Steffensen, J.P., Dahl-Jensen, D., Vinther, B.M., Clausen, H.B., 2006. The Greenland Ice Core Chronology 2005, 15-42 ka. Part 1: constructing the time scale. Quaternary Science Reviews 25, 3246-3257.

Arboleya, M-L., Babault, J., Owen, L.A., Teixell, A., Finkel, R.C., 2008. Timing and nature of Quaternary fluvial incision in the Ouarzazate forleland basin, Morocco. Journal of the Geological Society 165, 1059-1073.

Awad, H., 1963. Some aspects of the geomorphology of Morocco related to the Quaternary climate. *The Geographical Journal*, 129, 129-139.

Bakke, J., Lie, Ø., Heegaard, E., Dokken, T., Haug, G.H., Birks, H.H., Dulski, P., 2009. Rapid oceanic and atmospheric changes during the Younger Dryas cold period. Nature Geoscience 2, 202-205.

Balco, G., Stone, J.O., Lifton, N.A., Dunai, T.J., 2008. A complete and easily accessible means of calculating surface exposure ages or erosion rates from $^{10}$Be and $^{26}$Al measurements. Quaternary Geochronology 3, 174-195.

Balco, G., Briner, J., Finkel, R.C., Rayburn, J.A., Ridge, J.C., Schaefer, J.M., 2009. Regional beryllium-10 production rate calibration for late-glacial northeastern North America. Quaternary Geochronology 4, 93-107.

Ballantyne, C.K., 2007. Loch Lomond Stadial glaciers in North Harris, Outer Hebrides, North-West Scotland: glacier reconstruction and palaeoclimatic implications. Quaternary Science Reviews 26, 3134-3149.

Bard, E. Abrupt climate changes over millennial timescales: Climate shock. Physics Today 55, 32-38.

Barsch, D., 1996. Rockglaciers: Indicators for the Present and Former Geoecology in High Mountain Environments. Springer Verlag: Berlin.

Berger, A., Loutre, M.F., 1991. Insolation values for the climate of the last 10 million years. Quaternary Science Reviews 10, 297-317.

Blome, M.W., Cohen, A.S., Tryon, C.A., Brooks, A.S., Russell, J., The environmental context for the origins of modern human diversity: A synthesis of regional variability in African climate 150,000-30,000 years ago. Journal of Human Evolution 62, 563-592.

Boulton, S.J., Stokes, M., Mather, A.E., 2014. Transient fluvial incision as an indicator of active faulting and Plio-Quaternary uplift of the Moroccan High Atlas. Tectonophysics 633, 16-33.

Calvet, M., Delmas, M., Gunnell, Y., Braucher, R., Bourlès, D., 2011. Recent advances in research on Quaternary glaciations in the Pyrenees. In: Ehlers, J., Gibbard, P.L., Hughes, P.D. (Eds.), Quaternary Glaciations — Extent and Chronology: A Closer Look. Developments in Quaternary Science, 15. Elsevier, Amsterdam, pp. 127–140.

Célerier, J., Charton, A., 1922. Sur la présence de formes glaciaires dans le Haut Atlas de Marrakech: Hespéris 2, 373-384.

Célerier, J., and Charton, A., 1923, Un lac d'origine glaciaire dans le Haut Atlas (lac d'Ifni). Hespéris 3, 501–513.

Chardon,M., & Riser, J., 1981. Formes et processus géomorphologiques dans le Haut-Atlas marocain. *Revue de Géographie Alpine*, 69, 561-582.

Child, D., Elliott, G., Misfud, C., Smith, A.M., Fink, D., 2000. Sample processing for Earth science studies at ANTARES. Nuclear Instruments and Methods B172, 856–860.

Choubert, G., Joly, F., Gigout, M., Marçais, J., Margat, J., Raynal, R., 1956. Essai de classification du Quaternaire continental du Maroc. Comptes Rendus des Séances de l'Académie des Sciences, Paris 243, 504-506.

Çiner, A., Sarıkaya, M.A., Yıldırım, C. 2015. Late Pleistocene piedmont glaciation in the Eastern Mediterranean; insights from cosmogenic $^{36}$Cl dating of hummocky moraine in southern Turkey. Quaternary Science Reviews 115, 44-56.

Clark, C.D., Hughes, A.L.C., Greenwood, S.L., Jordan, C., Sejrup, H.P., 2012. Pattern and timing of retreat of the last British–Irish Ice Sheet. Quaternary Science Reviews 44, 112–146.

Delcaillau, B., Lavilee, E., Amhrar, M., Namous, M., Dugué, O., Pedoja, K., 2010. Quaternary evolution of the Marrakech High Atlas and morphotectonic evidence of activity along the Tizi N'Test Fault, Morocco. Geomorphology 118, 262-279.

Delcaillau, B., Amrhar, M., Namous, M., Laville, E., Pedoja, K., Dugué, O., 2011. Transpressional tectonics in the Marrakech High Atlas: Insight by the geomorphic evolution of drainage basins. Geomorphology 134, 344-362.

Delcaillau, B., Dugué, O., Namous, M., Pedoja, K., Mostafa, A., Laville, E., 2016. Pleistocene fluviatile deposits in the Ourika drainage basin (Marrakech High Atlas, Morocco): indicators of climatic variations associated with base level change. Zeitschrift für Geomorphologie 60, 131-150.

De Martonne, E.,1924. Les formes glaciaires sur le versant Nord du Haut Atlas: Annales de Géographie (Paris, 15 Mai 1924), v. 183, p. 296-302.

de Menocal, P.B., 2008. Africa on the edge. *Nature Geoscience*, 1, 650-651.

Di Nicola, L., Schnabel, C., Wilcken, K.M., Gméling, K. 2009. Determination of chlorine concentrations in whole rock: Comparison between prompt-gamma activation and isotope-diultion AMS analysis. Quaternary Geochronology 4, 501-507.

Dresch, J., 1941. Recherches sur l'évolution du relief dans le Massif Central du Grand Atlas le Haouz et le Sous: Arrault et Cie, Maitres Imprimeurs. Tours. 653 pp.

Dresch, J., 1949. Sur des formations de remblaiement continental et la présence de formes glaciaires dans le Haut Atlas calcaire. Comptes Rendus Sommaire des Séances de la Société Géologique de France, 9-10, 169-171.

Dresch, J., Raynal, R., 1953. Les formes glaciaires et périglaciaires dans le Moyen Atlas. Comptes Rendus Sommaire des Séances de la Société Géologique de France, 11/12, 195-197.

Dunne, J., Elmore, D., Muzikar, P.. 1999. Scaling factors for the rates of production of cosmogenic nuclides for geometric shielding and attenuation at depth on sloped surfaces. Geomorphology 27, 3-11.

El Alami, S.O., Tadili, B., Aït Brahim, L., Mouayn, I., 2004. Seismicity of Morocco for the Period 1987-1994. Pure and Applied Geophysics 161, 969-982.

Fink, D., Smith, A., 2007. An inter-comparison of $^{10}$Be and $^{26}$Al AMS reference standards and the $^{10}$Be half-life, Nuclear Instruments and Methods B259, 600-609.

Fink, D., McKelvey, B., Hannan, D., Newsome, D. 2000, Cold rocks, hot sands: In-situ cosmogenic applications in Australia at ANTARES: Nuclear Instruments and Methods in Physics Research B172, 838–846.

Fletcher, W.J., Hughes, P.D., 2017. Anthropogenic triggers for Late Holocene soil erosion in the Jebel Toubkal, High Atlas, Morocco. Catena 149, 713-726. http://doi.org/10.1016/j.catena.2016.03.025

Frödin, J. 1922. Géographie physique de l'Ouest du Maroc. Geografiska Annaler 1922, 58-76.

Giraudi, C., Bodrato, G., Ricci Lucchi, M., Cipriani, N., Villa, I.M., Giaccio, B., Zuppi, G.M. 2011. The Middle and Late Pleistocene glaciations in the Campo Felice basin (Central Apennines, Italy). *Quaternary Research*, 75, 219-230.

Glasser, N.F., Hughes, P.D., Fenton. C.R., Schnabel, C. and Rother, H. (2012) $^{10}$Be and $^{26}$Al exposure-age dating of bedrock surfaces on the Aran Ridge, Wales: Evidence for a thick Welsh Ice Cap at the LGM. *Journal of Quaternary Science* 27, 97-104.

Gromig, R., Mechernich, S., Ribolini, A.,Wagner, B., Zanchetta, G., Isola, I., Bini, M., Dunai, T.J., 2017. Evidence for a Younger Dryas deglaciation in the Galicica Mountains (FYROM) from cosmogenic $^{36}$Cl. Quaternary International. http://dx.doi.org/10.1016/j.quaint.2017.07.013

Hannah, G., Hughes, P.D., Gibbard, P.L., 2016. Pleistocene plateau ice fields in the High Atlas, Morocco. In: Hughes, P. D. & Woodward, J. C. (ed.) Quaternary Glaciation in the Mediterranean Mountains. Geological Society, London, Special Publications 433, 25-53. http://doi.org/10.1144/SP433.12

Heybrock, W., 1953. Eiszeitliche Gletscherspuren und heutige Schneeverhältnisse im Zentralgebiet des Hohen Atlas. Zeitschrift für Gletscherkunde und Glazialgeologie, 2, 317-321.

Heyman, J. 2014. Paleoglaciation of the Tibetan Plateau and surrounding mountains based on exposure ages and ELA depression estimates, Quaternary Science Reviews 91, 30-41.

Hooker, J.D., Ball, J., 1878. Journal of a tour in Marocco and the Great Atlas, with an appendix including a sketch of the geology of Marocco, by George Maw. Macmillan & Co. London. 499 pp.

Hughes, P.D., 2009. Twenty-first Century Glaciers in the Prokletije Mountains, Albania. Arctic, Antarctic and Alpine Research 41, 455-459.

Hughes, P.D., 2010. The role of geomorphology in Quaternary stratigraphy: morphostratigraphy, lithostratigraphy and allostratigraphy. Geomorphology 123, 189-199.

Hughes, P.D. 2014. Little Ice Age glaciers in the Mediterranean mountains. Mediterranée 122, 63-79.

Hughes, P.D., 2018. Little Ice Age glaciers and climate in the Mediterranean mountains: a new analysis. Cuadernos de Investigación Geográfica. http://dx.doi.org/10.18172/cig.3362

Hughes, P.D., Gibbard, P.L. 2015. A stratigraphical basis for the Last Glacial Maximum (LGM). Quaternary International 383, 174-185.

Hughes, P.D., Woodward, J.C. 2008. Timing of glaciation in the Mediterranean mountains during the last cold stage. Journal of Quaternary Science 23, 575-588.

Hughes, P.D., Woodward, J.C., 2016. Quaternary Glaciation in the Mediterranean Mountains: A New Synthesis. In: Hughes, P.D., Woodward, J.C. (2016) Quaternary glaciation in the Mediterranean Mountains. Geological Society of London Special Publications 433, 1-23. https://doi.org/10.1144/SP433.14

Hughes, P.D., Gibbard, P.L., Woodward, J.C., 2004. Quaternary glaciation in the Atlas Mountains, North Africa. In: Ehlers, J., Gibbard, P.L., (Eds) *Quaternary Glaciation - Extent and Chronology. Volume 3: Asia, Latin America, Africa, Australia, Antarctica*. Amsterdam: Elsevier. p. 255-260.

Hughes, P.D., Woodward, J.C., Gibbard, P.L., Macklin, M.G., Gilmour, M.A., Smith G.R., 2006. The glacial history of the Pindus Mountains, Greece. Journal of Geology 114, 413-434.

Hughes, P.D., Fenton, C.R., Gibbard, P.L. 2011a. Quaternary glaciations of the Atlas Mountains, North Africa. In: Ehlers, J., Gibbard, P.L. and Hughes, P.D. (Eds) Quaternary Glaciations - Extent and Chronology, Part IV - A Closer Look. Amsterdam: Elsevier. p. 1071-1080.

Hughes, P.D., Woodward, J.C., van Calsteren, P.C., Thomas, L.E., 2011b. The Glacial History of The Dinaric Alps, Montenegro. Quaternary Science Reviews 30, 3393-3412.

Hughes, P.D., Fink, D., Fletcher, W.J., Hannah, G. 2014. Catastrophic rock avalanches in a glaciated valley of the High Atlas, Morocco: $^{10}$Be exposure ages reveal a 4.5 ka seismic event. Geological Society of America Bulletin 126, 1093-1104.

Lefèvre, D. and Raynal, J-P., 2002. Les Formations Plio-Pléistocènes de Casablanca et la Chronostratigraphie du Quaternaire Marin du Maroc Revistées. Quaternaire 13, 9-21.

Lewis, C.J., McDonald, E.V., Sancho, C., Peña, J.L., Rhodes, E.J., 2009, Climatic implications of correlated Upper Pleistocene glacial and fluvial deposits on the Cinca and Gállego Rivers (NE Spain) based on OSL dating and soil stratigraphy. Global and Planetary Change 67, 141-152.

Lohne, Ø., Mangerud, J., Svendsen, J.I., 2012. Timing of the Younger Dryas glacial maximum in western Norway. Journal of Quaternary Science 27, 81-88.

Marrero, S.M., Phillips, F.M., Borchers, B., Lifton, N., Aurner, R., Balco, G., 2016. Cosmogenic nuclide systematics and the CRONUScalc scale. Quaternary Geochronology 31, 160-187.

Mather, A.E., Stokes, M., 2017. Bedrock structural controls on catchment-scale connectivity and alluvial fan processes, High Atlas Mountains, Morocco. In: Ventra, D., Clarke, L.E., (eds) Geology and Geomorphology of Alluvial Fans: Terrestrial and Planetary Perpectives. Geological Society, London, Special Publications 440. http://dx.doi.org/10.1144/SP440.15

Mensching, H., 1953. Morphologische Studien im Hohen Atlas von Marokko. Würzburger Geographica Arbeiten, H.1, 104 pp.

Mensching, H., 1960. Bericht und Gedanken zur Tagung der Kommission für Periglazialforschung in der IGU in Marokko vom 19. bis 31. Oktober 1959. *Zeitschrift für Geomorphologie*, N.F. 4, 159-170.

Messerli, B., 1967. Die eiszeitliche und die gegenwartige Vertgletscherung im Mittelemeeraum. Geographica Helvetica, 22, 105-228.

Messerli, B., Winiger M., 1992. Climate, environmental change and resources of the African mountains from the Mediterranean to the Equator: Mountain Research and Development, v. 12, p. 315-336.

Mifsud, C., Fujioka, T., Fink, D., 2013. Extraction and purification of quartz in rock using hot-phosphoric acid for in situ cosmogenic exposure dating, Nuclear Instruments and Methods B294, 203-207.

Miller, M.S., Becker, T.W., 2013. Reactivated lithosperic-scale discontinuities localize dynamic uplift of the Moroccan Atlas Mountains. Geology 42, 335-38.

Neltner, L., 1938. Etudes géologiques dans le sud marocain (Haut-Atlas et Anti-Atlas). Notes et Mémoires, Service Géologique du Maroc 42, 1-298.

Nishiizumi, K., Imamura, M., Caffee, M.W., Southon, J.R., Finkel, R.C., and McAninch, J., 2007, Absolute calibration of $^{10}$Be AMS standards: Nuclear Instruments and Methods in Physics Research B 258, p. 403-413.

Orientazion, 2006. Toubkal & Marrakech, Hiking Map, 1;50,000. Orientazion (later edition in 2008 published by Cordee).

Phillips, F.M., Marrero, S., Stone, J.O., Lifton, N.A. 2012. Chlorine-36 Production Rate Calibration by the CRONUS-Earth Project. American Geophysical Union, Fall Meeting 2012, abstract #EP13C-0851.

Palacios, D., Marcos, J., Vázquez-Selem, L. 2011. Last Glacial Maximum and deglaciation of Sierra de Gredos, central Iberian Peninsula. Quaternary International, 233, 16-26.

Palacios, D., Andres, N. de, Marcos, J. De, Vázquez-Selem, L., 2012. Glacial landforms and their paleoclimatic significance in Sierra de Guadarrama, Central Iberian Peninsula. Geomorphology 139-140.

Pope, R.J., Hughes, P.D., Skourtsos, E. 2016. Glacial history of Mt Chelmos, Peloponnesus, Greece. In: Hughes, P. D. & Woodward, J. C. (ed.) Quaternary Glaciation in the Mediterranean Mountains. Geological Society, London, Special Publications, 433. doi.org/10.1144/SP433.11

Pouclet, A., Aarab, A., Fekkak, A., Benharraf, M., 2007. Geodynamic evolution of the northwestern Paleo-Gondwanan margin in the Morocco Atlas at the PreCambrian-Cambrian boundary. *Geological Society of America, Special Publication*, 423, 27-60.

Raynal, R., Dresch, J., Joly, F. (1956). Deux exemples régionaux de glaciation quaternaire au Maroc: Haut Atlas Oriental, Moyen Atlas Septentrional. *IV Congrès INQUA, Rome-Pisa,* p. 108-117.

Rolfe, C.J., Hughes, P.D., Fenton, C.R., Schnabel, C., Xu, S., Brown, A.G. (2012) Paired $^{10}$Be and $^{26}$Al exposure ages from Lundy: new evidence for the extent and timing of Devensian glaciation in the southern British Isles. Quaternary Science Reviews 43, 61-73.

Schimmelpfennig, I., Benedetti, L., Finkel, R., Pik, R., Blard, P.H., Bourles, D., Burnard, P., and Williams, A., 2009, Sources of in-situ Cl-36 in basaltic rocks. Implications for calibration of production rates: Quaternary Geochronology 4, 441-461.

Serrano, E., González-Trueba, J.J., Pellitero, R., Gómez-Lende, M., 2016. Quaternary glacial history of the Cantabrian Mountains of northern Spain: a new synthesis. In: Hughes, P. D. & Woodward, J. C. (ed.) Quaternary Glaciation in the Mediterranean Mountains. Geological Society, London, Special Publications, 433. doi:10.1144/SP433.8

Stokes, M., Mather, A.E., Belfoul, A., Farik, F., 2008. Active and passive tectonic controls for transverse drainage and river gorge development in a collisional mountain belt (Dades Gorges, High Atlas Mountains, Morocco). Geomorphology 102, 2-20.

Stokes, M., Mather, A.E., 2015. Controls on modern tributary-junction alluvial fan occurrence and morphology: High Atlas Mountains, Morocco. Geomorphology 248, 344-362.

Stokes, M., Mather, A.E., Belfoul, M., faik, F., Bouzid, S., geach, M.R., Cunha, P.P., Boulton, S.J., Thiel, C., Controls on dryland mountain landscape development along the NW Saharan desert margin: Insights from Quaternary terrace sequences (Dadès River, south-central High Atlas, Morocco). Quaternary Science Reviews 166, 363-379.

Svensson, A., Andersen, K.K., Bigler, M., Clausen, H.B., Dahl-Jensen, D., Davies, S.M., Johnsen, S.J., Muscheler, R., Parrenin, F., Rasmussen, S.O., Röthlisberger, R., Seierstad, I., Steffensen, J.P., Vinther, B.M., 2008. A 60 000 year Greenland stratigraphic ice core chronology. Climate of the Past, 4, 47-57.

Thompson, J. 1899. The Geology of Southern Morocco and the Atlas Mountains. Quarterly Journal of the Geological Society 55, 190-213.

Tjallinghii, R., Claussen, M., Stuut, J-B. W., Fohlmesiter, J., Jahn, A., Bickert, T., Lamy, F., Röhl, U., 2008. Coherent high- and low-latitude controls on the northwest African hydrological balance. Nature Geoscience 1, 670-675.

Vieira, G., Mora, C., Faleh, A., 2017. Ground surface temperatures indicate the presence of permafrost in North Africa (Djebel Toubkal, High Atlas, Morocco). The Cryosphere 11, 1691-1705. https://doi.org/10.5194/tc-11-1691-2017

Vogt, S., Wang, M.S., Li, R., Lipschutz, M., 1994. Chemistry operations at Purdue's accelerator mass spectrometry facility, Nuclear Instruments & Methods in Physics Research B92,153.

Wiche, K., 1953. Klimamorphologische und talgeschichtliche Studien im M'Goungebiet. Mitteilungen Der Geographischen Gesellschaft Wien 95, 4-41.

World Meteorological Organisation, 1998. 1961-1990 global climate normals. Electronic resource. National Climatic Data Center, US: Asheville, NC. (CD-ROM).

Woodward, J.C., Lewin, J., Macklin, M.G. 1992. Alluvial sediment sources in a glaciated catchment: the Voidomatis basin, northwest Greece. Earth Surface Processes and Landforms 16, 205-216.

Woodward, J.C. and Hughes, P.D. (2011) Glaciation in Greece: a new record of cold stage environments in the Mediterranean. In: Ehlers, J., Gibbard, P.L. and Hughes, P.D. (eds), Quaternary Glaciations – Extent and Chronology, Part IV – A Closer Look. Amsterdam: Elsevier: pp. 175–198.

Woodward, J.C., Macklin, M.G., Smith, G.R. 2004. Pleistocene Glaciation in the Mountains of Greece. In Ehlers, J. and Gibbard, P.L. (eds) *Quaternary Glaciations - Extent and Chronology. Part I: Europe*. Elsevier. p. 155-173.

Woodward, J.C., Hamlin, R.H.B., Macklin, M.G., Hughes, P.D., Lewin, J., 2008. Glacial activity and catchment dynamics in northwest Greece: longterm river behaviour and the slackwater sediment record for the last glacial to interglacial transition. Geomorphology 101, 44-67.

**Figures**

**Figure 1.** Extent of ice in the Toubkal massif during the most extensive recorded glaciation. The three regions sampled for cosmogenic dating are indicated by white rectangles. Glacier limits have been determined by field observations in most areas and supplemented by satellite images for the southeastern sector.

**Figure 2.** Geological map of the study area. Adapted from Dresch (1941).

**Figure 3.** Glacial geomorphological map of the seven glaciated valleys defined by Region 1 which covers the northern slopes of Azrou n'Tamadot (3770 m a.s.l.). Aksoual (3912 m a.s.l.) and Bou Iguenouane (3877 m a.s.l.). The five easternmost glacial valleys drain into Assif n'Imenane , and the two westernmost drain into Assif Ait Mizane. Locations of cosmogenic sampling for exposure dating are given by alphabetic characters. Mapped moraines, labelled as Unit 1, 2 and 3, are grouped intime-stratigraphical order from oldest to youngest based on their respective exposure ages distributions (see text for details).

**Figure 4.** Glacial geomorphological map of the Azib Mzik valley defined by Region 2 on the northern slopes of Adrar el Hajj (3129 m a.s.l.). Sample sites and moraine stratigraphy as described for Fig 3.

**Figure 5.** Glacial geomorphological map of the central Toubkal massif (4167 m a.s.l.) defined by Region 3. Cosmogenic sampling was restricted to the lower reaches of the Aït Mizane valley below Sidi Chamarouch. Identification of moraine Units-1, -2 and -3 as prescribed for Regions 1 and 2 (see Figures 3 and 4) are not available due to a paucity of samples for cosmogenic dating which requires further reconnaissance and mapping.

**Figure 6.** Striated clasts in the moraines of the High Atlas. A: Assif n'Imserdane; B: Aït Mizane valley (near Sidi Shamarouch); C: Aït Mizane valley (lowest moraine); D: exposed section through till containing numerous striated clasts in the lower Iguenouane valley near the village of Tacheddirt.

**Figure 7.** Moraines on the western flank of the lower Irhzer Tamda draining into the Imenane Valley. The boulder ridge in this picture are Unit-2 moraines and a sample from a large boulder

(4x8x6 m) (IT-10; C) has yielded a $^{36}$Cl exposure age of **29.5 ± 1.7 ka**. The mountain in the background is Aksoual (3912 m a.s.l.). Photo looking due south.

**Figure 8.** Photo looking up valley (due south) towards Tizi Likemt (3555 m a.s.l.) in in Irhzer n'Likemt showing the crests (red dashed lines) of Unit-3 moraine (higher elevation) and Unit-2 moraine. Unit-3 moraine is in cirque-like position below the backwall cliffs yielding two exposure ages of **13.7 ± 0.8** (Irhzwe-8; Q) and **12.1 ± 0.8** (Irhzwe-1; P) ka. Unit-2 moraines appear as flanking laterals with exposure ages of **16.6 ± 0.8** (Irhwze-3; N) ka and an outlier age of **8.9 ± 0.6 ka** (Irhwze-4; M).

**Figure 9.** The subangular/subrounded striated boulder Amguedoul-1 (R), perched on the crest of a Unit-1 (oldest) moraine in Amguedoul Valley, gave a $^{36}$Cl age of **80.0 ± 12.1 ka**. The boulder is located on the lowest elevation and most distal down-valley moraine. A second boulder at the same location (R), Amguedoul-7, gave an outlier $^{10}$Be age of **12.6 ± 0.8 ka**. Along the same moraine crest, approximately 100 m distance, a third boulder, Amguedoul-2 (S) gave a $^{10}$Be age of **87.9 ± 4.7** ka.

**Figure 10.** Truncated spur in the upper Aït Mizane valley near Sidi Chamarouch of Region-3 ( see fig 5. Note the perched erratic boulder on the foreground rock surface. A quartz-rich bedrock sample from the foreground area (Toubkal-1;AD) yielded a $^{10}$Be age of **52.0 ± 3.1 ka**.

**Figure 11**. Large subangular/subrounded boulder at c. 2010 m altitude near the lowest moraines of the Aït Mizane valley (Figure 5). A sample from the top of this boulder (Toubkal-4) yielded a $^{36}$Cl age of **50.0 ± 4.9** ka.

**Figure 12**. The mean exposure ages (and uncertainty at 1 SD) of the exposure ages from moraines in the High Atlas with reference to wider environmental changes in the North Atlantic region and NW Africa. The mean ages for the youngest two sets of moraines have small uncertainities and can viewed with confidence. However, the oldest moraines have considerable scatter and interpretations of the true age of the moraines is problematic (see text for details). The Greenland ice core data is based on the GICC05 age model (Andersen et al., 2006; Svensson et al. 2008). Sea surface temperature data from the North Atlantic Ocean based on alkenones (37-carbon) from core MD95 2042 off the southwestern Iberian margin (Bard 2002). The continental humidity index is from core GeoB7920-2 off the coast of NW Africa (from Tjallinghii et al. 2008); Insolation at 30°N in the northern hemisphere is from Berger and Loutre (1991).

**Tables**

**Table 1.** Valley morphometry data for the nine glaciated valleys in this study.

**Table 2.** Sample site data (all samples).

**Table 3.** $^{10}$Be isotope data.

**Table 4.** $^{36}$Cl isotope and major element geochemistry data (see Supplementary Tables for full geochemistry data).

**Table 5.** Relative $^{36}$Cl production (see Supplementary Tables for full datasets).

**Table 6.** Glacial phases showing $^{10}$Be and $^{36}$Cl ages grouped by stratigraphical unit (3 = youngest and highest moraines, 1 = oldest and lowest moraines).

**Supplementary Tables**

**Supplementary Table 1**. Input file for $^{10}$Be exposure ages via the CRONUS calculator (Balco et al. 2008; 2009).
(http://hess.ess.washington.edu/math/al_be_v22/alt_cal/Balco_NENA_age_input.html).

**Supplementary Table 2**. Input file for the $^{36}$Cl exposure ages via CRONUScalc website calculator (http://cronus.cosmogenicnuclides.rocks/2.0/html/cl/).

**Supplementary Table 3**. Output file for the $^{36}$Cl exposure ages via CRONUScalc website calculator (http://cronus.cosmogenicnuclides.rocks/2.0/html/cl/).

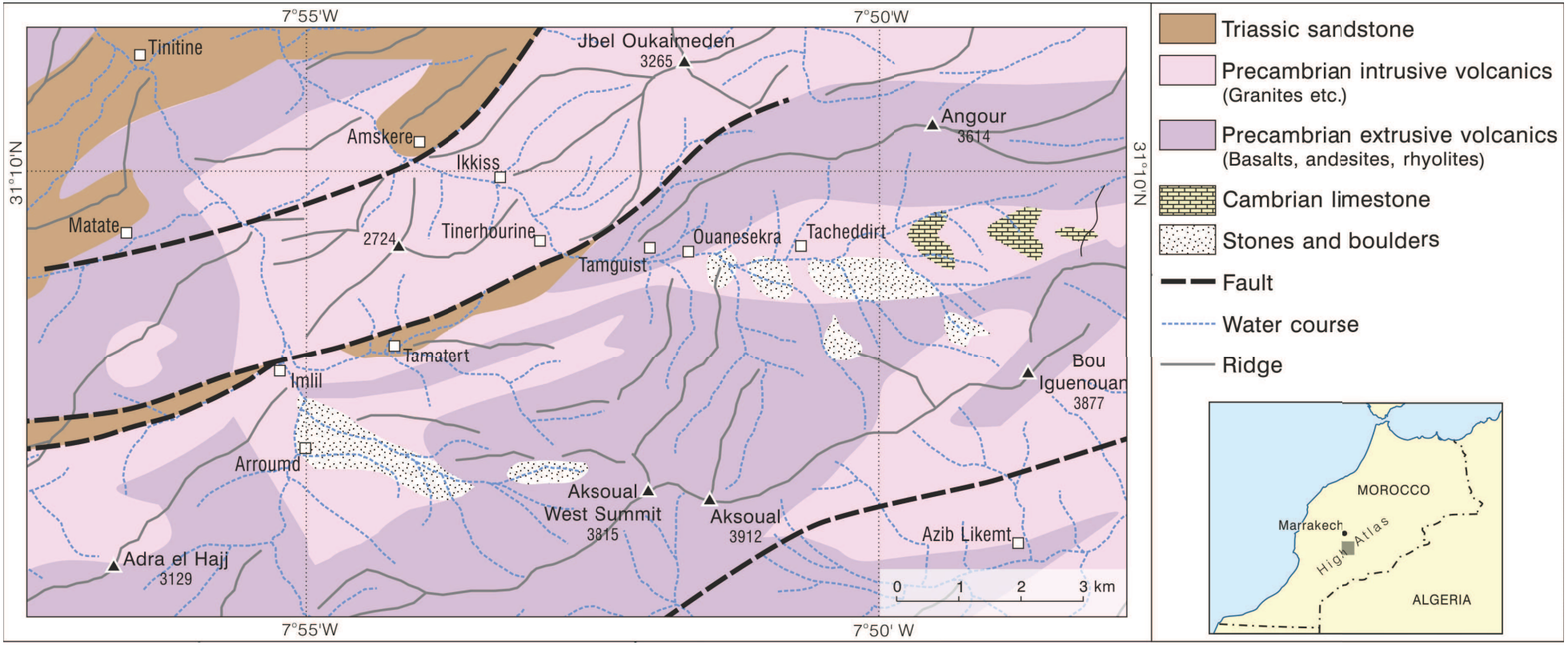
7°55'W
7°50'W
31°10'N
Tinitine
Jbel Oukaimeden
3265
Angour
3614
Amskere
Ikkiss
Matate
2724
Tinerhourine
Tamguist
Ouanesekra
Tacheddirt
Tamatert
Imlil
Bou
Iguenouan
3877
Arroumd
Aksoual
West Summit
3815
Aksoual
3912
Azib Likemt
Adra el Hajj
3129
0 1 2 3 km
7°55'W
7°50' W
31°10'N
Triassic sandstone
Precambrian intrusive volcanics
(Granites etc.)
Precambrian extrusive volcanics
(Basalts, andesites, rhyolites)
Cambrian limestone
Stones and boulders
Fault
Water course
Ridge
MOROCCO
Marrakech
High Atlas
ALGERIA

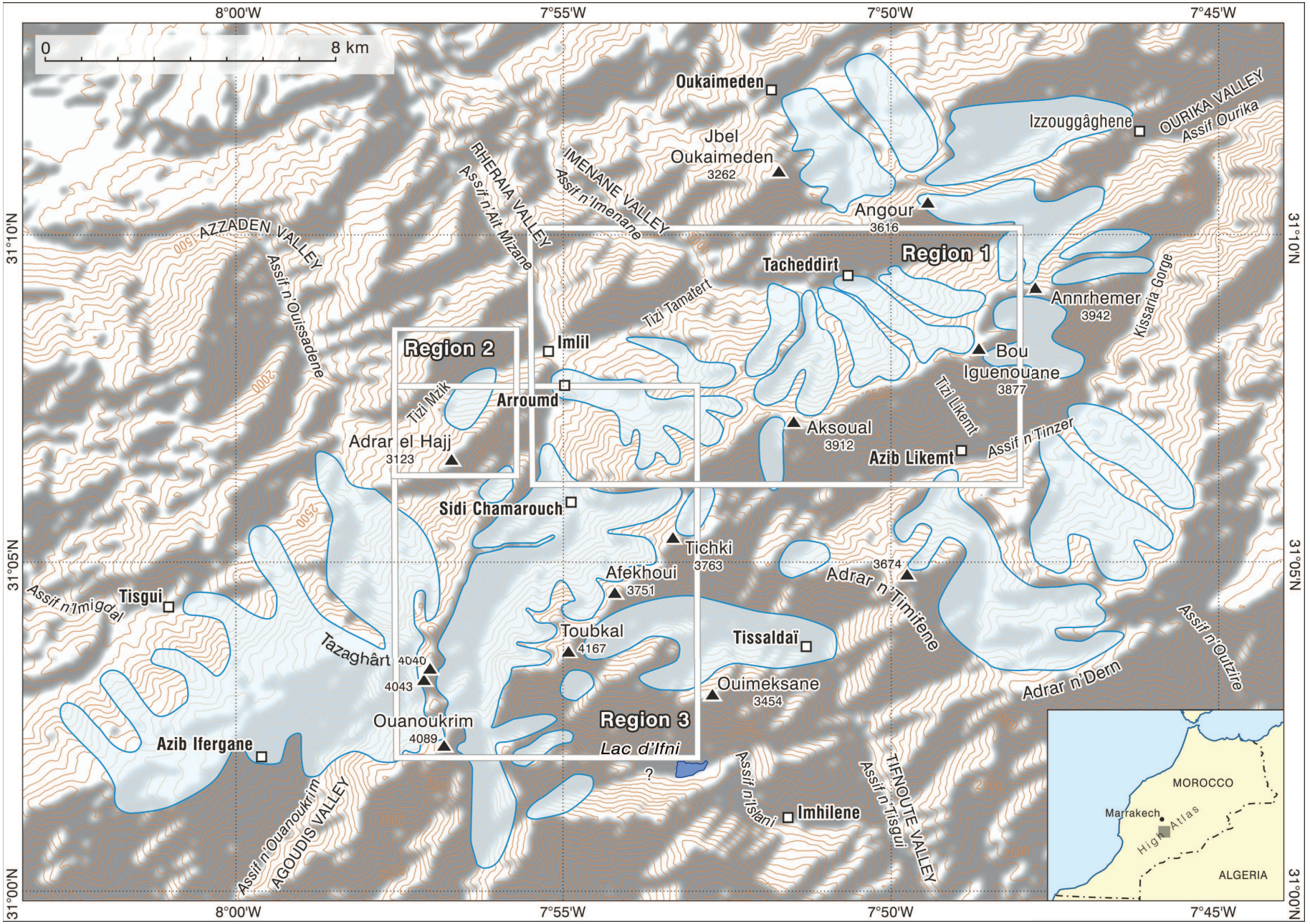
8°00'W
7°55'W
7°50'W
7°45'W
31°10'N
31°05'N
31°00'N
0
8 km
Oukaimeden
Izzouggâghene
OURIKA VALLEY
Assif Ourika
Jbel
Oukaimeden
3262
RHERAIA VALLEY
Assif n'Ait Mizane
IMENANE VALLEY
Assif n'Imenane
Angour
3616
AZZADEN VALLEY
Assif n'Ouissadene
Region 1
Tacheddirt
Annrhemer
3942
Kissaria Gorge
Tizi Tamatert
Region 2
Imlil
Bou
Iguenouane
3877
Tizi Likemt
Tizi Mzik
Arroumd
Adrar el Hajj
3123
Aksoual
3912
Azib Likemt
Assif n'Tinzer
Sidi Chamarouch
Tichki
3763
3674
Afekhoui
3751
Adrar n'Timirene
Tisgui
Assif n'Imigdal
Toubkal
4167
Tissaldaï
Assif n'Outzire
Tazaghârt
4040
4043
Ouimeksane
3454
Adrar n'Dern
Ouanoukrim
4089
Region 3
Lac d'Ifni
Azib Ifergane
Assif n'Ouanoukrim
AGOUDIS VALLEY
Assif n'Isiani
Imhilene
TIFNOUTE VALLEY
Assif n'Tisgui
MOROCCO
Marrakech
High Atlas
ALGERIA

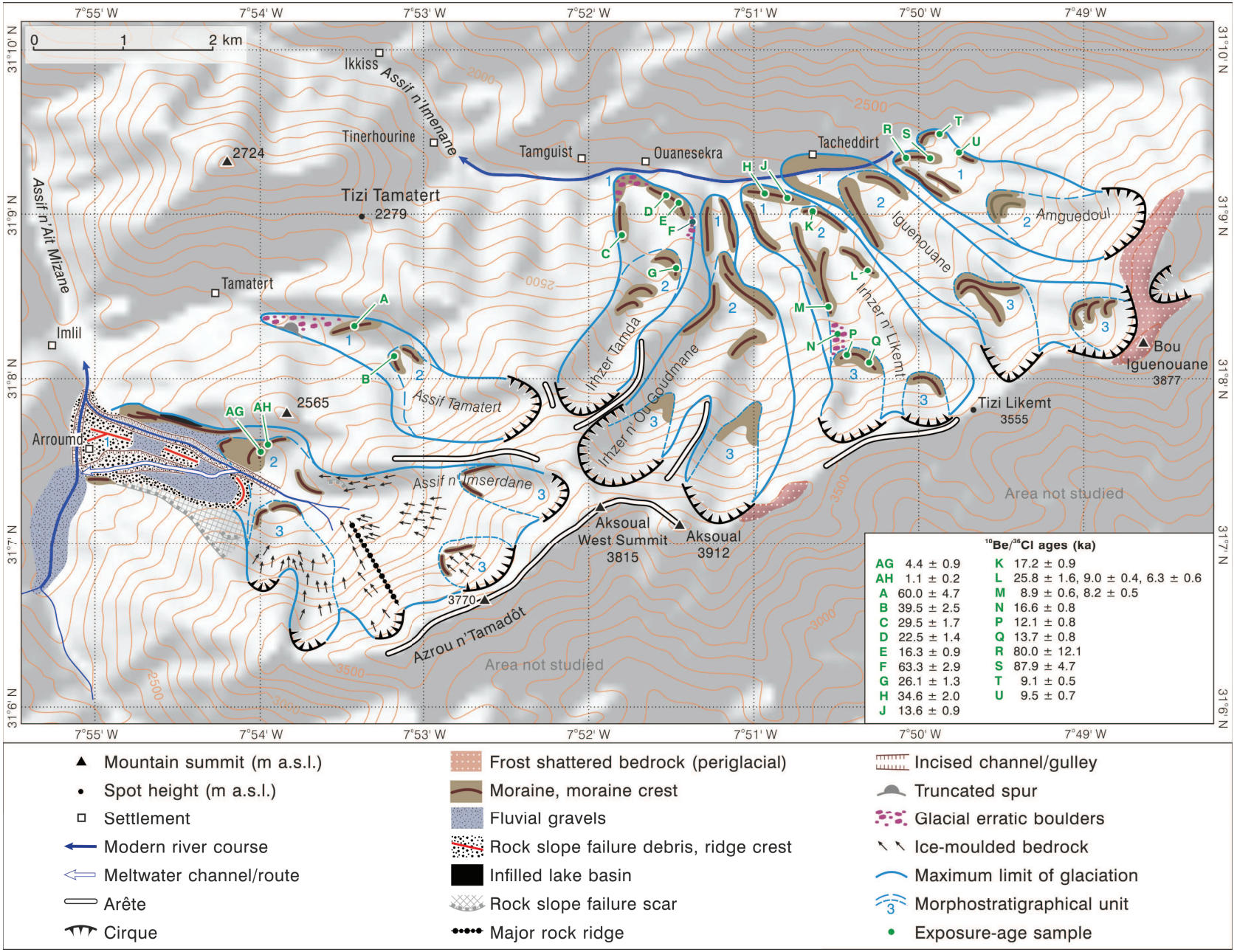
7°55' W
7°54' W
7°53' W
7°52' W
7°51' W
7°50' W
7°49' W
31°10' N
31°9' N
31°8' N
31°7' N
31°6' N
0 1 2 km
Ikkiss
Assif n'Imenane
Tinerhourine
Tamguist
Ouanesekra
Tacheddirt
2724
Tizi Tamatert
2279
Assif n'Ait Mizane
Tamatert
Imlil
Arroumd
2565
Assif Tamatert
Irhzer Tamda
Irhzer n' Ou Goudmane
Assif n' Imserdane
Aksoual West Summit
3815
Aksoual
3912
3770
Azrou n'Tamadôt
Area not studied
Iguenouane
Amguedoul
Irhzer n' Likemt
Tizi Likemt
3555
Bou Iguenouane
3877
2000
2500
3000
3500
A
B
C
D
E
F
G
H
J
K
L
M
N
P
Q
R
S
T
U
AG
AH
1
2
3
¹⁰Be/³⁶Cl ages (ka)
AG 4.4 ± 0.9
AH 1.1 ± 0.2
A 60.0 ± 4.7
B 39.5 ± 2.5
C 29.5 ± 1.7
D 22.5 ± 1.4
E 16.3 ± 0.9
F 63.3 ± 2.9
G 26.1 ± 1.3
H 34.6 ± 2.0
J 13.6 ± 0.9
K 17.2 ± 0.9
L 25.8 ± 1.6, 9.0 ± 0.4, 6.3 ± 0.6
M 8.9 ± 0.6, 8.2 ± 0.5
N 16.6 ± 0.8
P 12.1 ± 0.8
Q 13.7 ± 0.8
R 80.0 ± 12.1
S 87.9 ± 4.7
T 9.1 ± 0.5
U 9.5 ± 0.7
Mountain summit (m a.s.l.)
Spot height (m a.s.l.)
Settlement
Modern river course
Meltwater channel/route
Arête
Cirque
Frost shattered bedrock (periglacial)
Moraine, moraine crest
Fluvial gravels
Rock slope failure debris, ridge crest
Infilled lake basin
Rock slope failure scar
Major rock ridge
Incised channel/gulley
Truncated spur
Glacial erratic boulders
Ice-moulded bedrock
Maximum limit of glaciation
Morphostratigraphical unit
Exposure-age sample

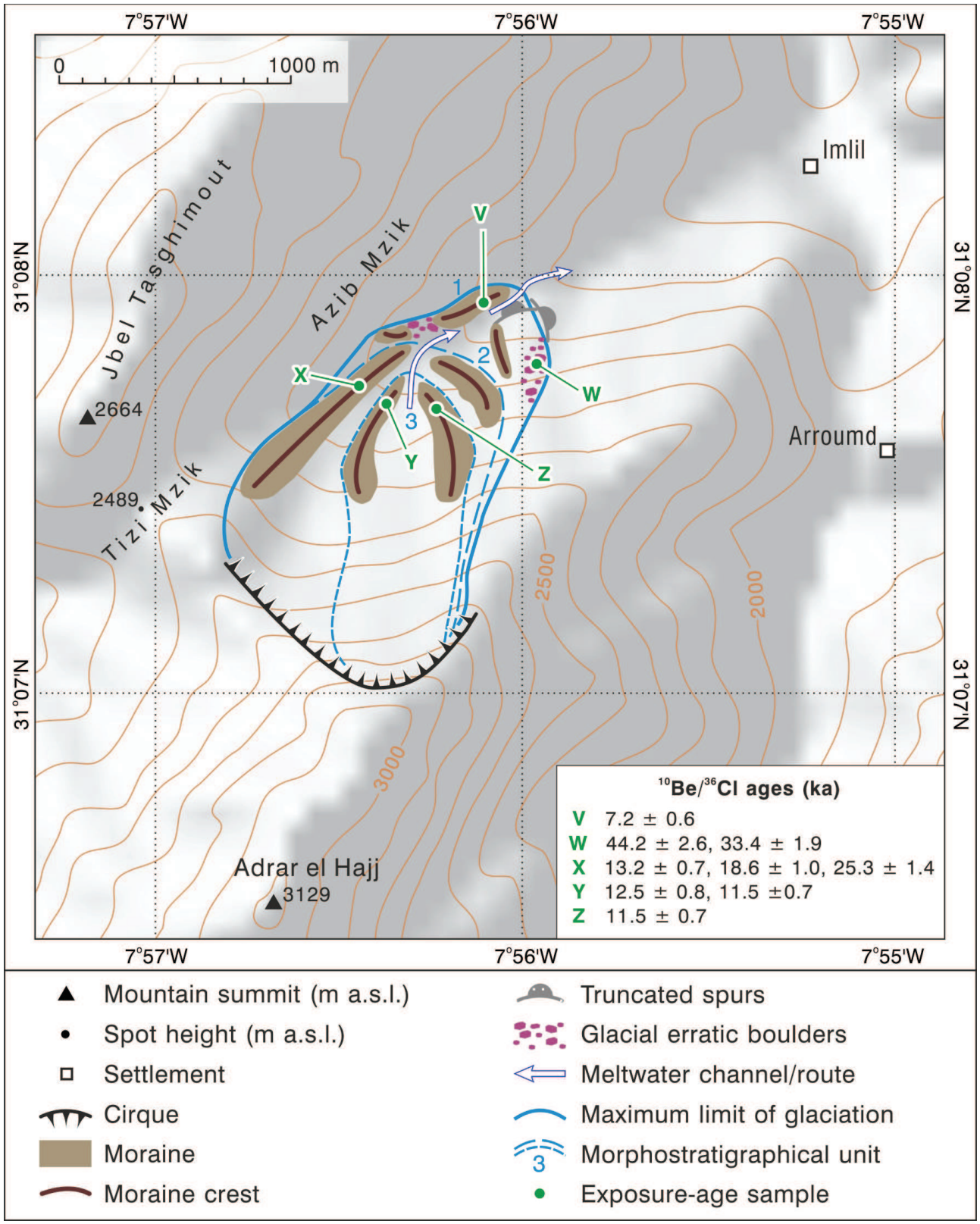
7°57'W
7°56'W
7°55'W
31°08'N
31°07'N
0
1000 m
Imlil
Jbel Tasghimout
Azib Mzik
Tizi Mzik
2664
2489
Arroumd
Adrar el Hajj
3129
2500
2000
3000
V
W
X
Y
Z
1
2
3
$^{10}$Be/$^{36}$Cl ages (ka)
V 7.2 ± 0.6
W 44.2 ± 2.6, 33.4 ± 1.9
X 13.2 ± 0.7, 18.6 ± 1.0, 25.3 ± 1.4
Y 12.5 ± 0.8, 11.5 ±0.7
Z 11.5 ± 0.7
Mountain summit (m a.s.l.)
Spot height (m a.s.l.)
Settlement
Cirque
Moraine
Moraine crest
Truncated spurs
Glacial erratic boulders
Meltwater channel/route
Maximum limit of glaciation
Morphostratigraphical unit
Exposure-age sample

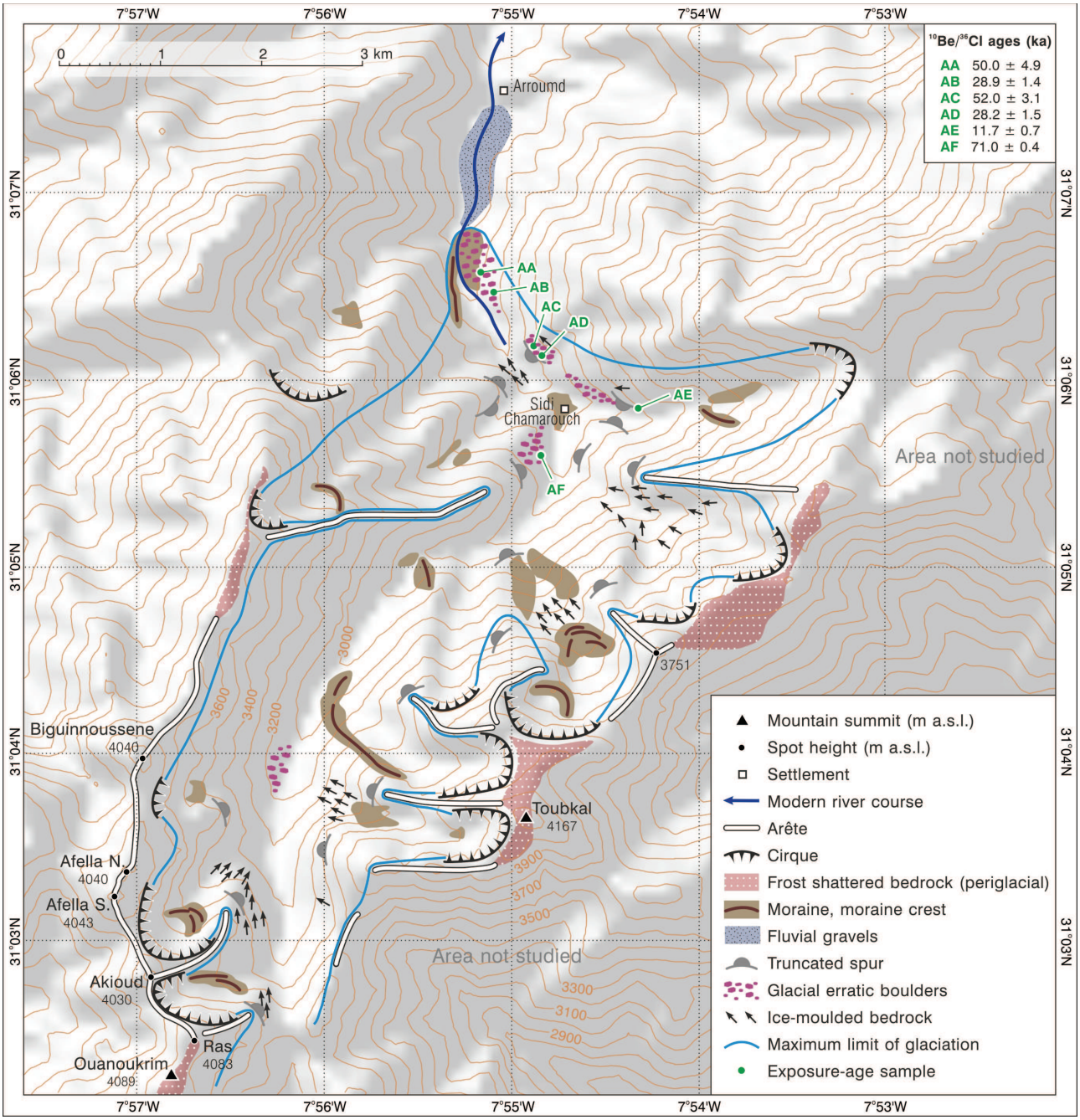
7°57'W
7°56'W
7°55'W
7°54'W
7°53'W
31°07'N
31°06'N
31°05'N
31°04'N
31°03'N
0
1
2
3 km
Arroumd
AA
AB
AC
AD
AE
AF
Sidi Chamarouch
Area not studied
3751
Biguinnoussene
4040
Toubkal
4167
Afella N.
4040
Afella S.
4043
Akioud
4030
Ras
4083
Ouanoukrim
4089
3600
3400
3200
3000
3900
3700
3500
3300
3100
2900
$^{10}$Be/$^{36}$Cl ages (ka)
AA 50.0 ± 4.9
AB 28.9 ± 1.4
AC 52.0 ± 3.1
AD 28.2 ± 1.5
AE 11.7 ± 0.7
AF 71.0 ± 0.4
Mountain summit (m a.s.l.)
Spot height (m a.s.l.)
Settlement
Modern river course
Arête
Cirque
Frost shattered bedrock (periglacial)
Moraine, moraine crest
Fluvial gravels
Truncated spur
Glacial erratic boulders
Ice-moulded bedrock
Maximum limit of glaciation
Exposure-age sample


IT-10; C

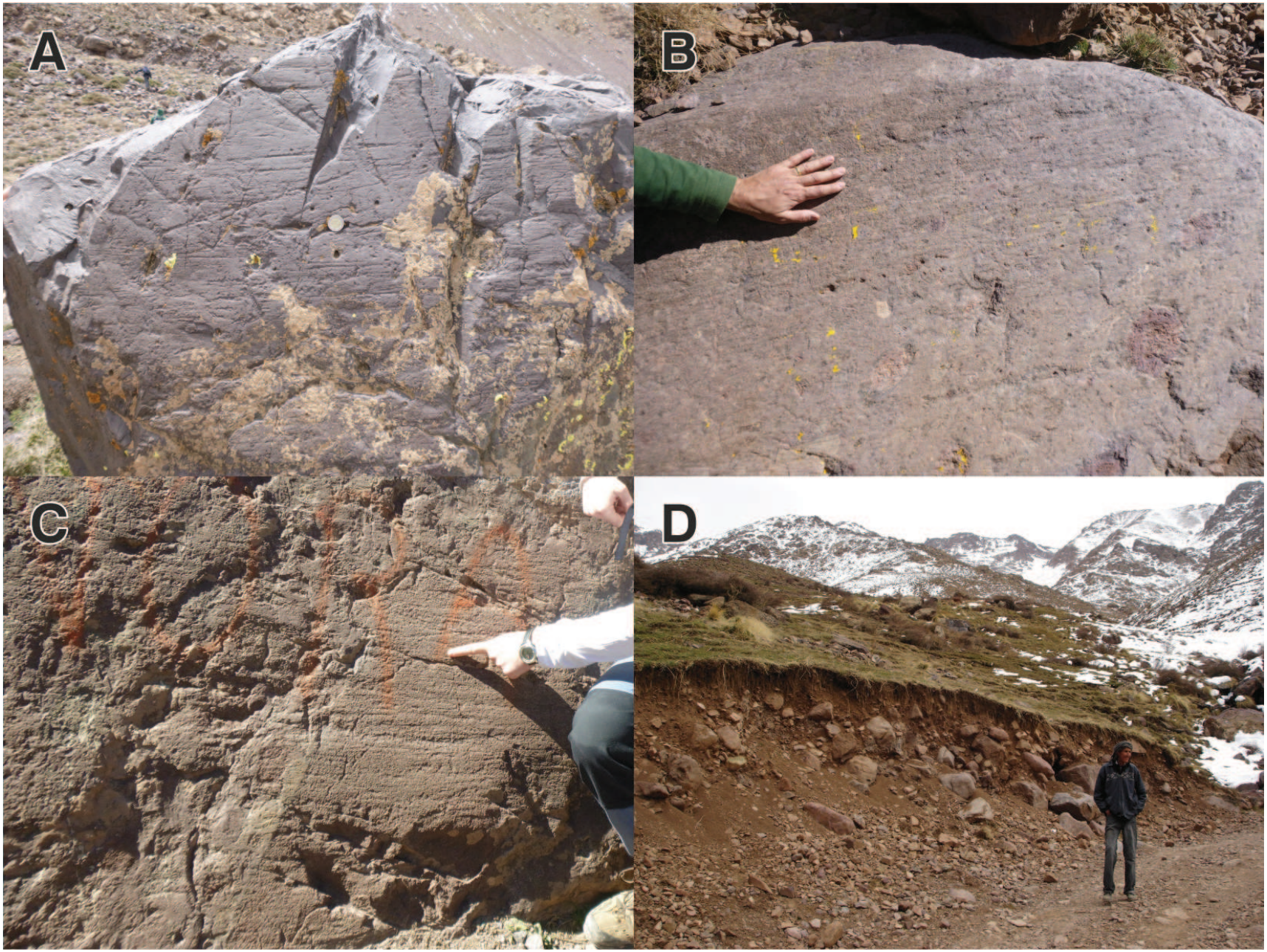
A
B
C
D

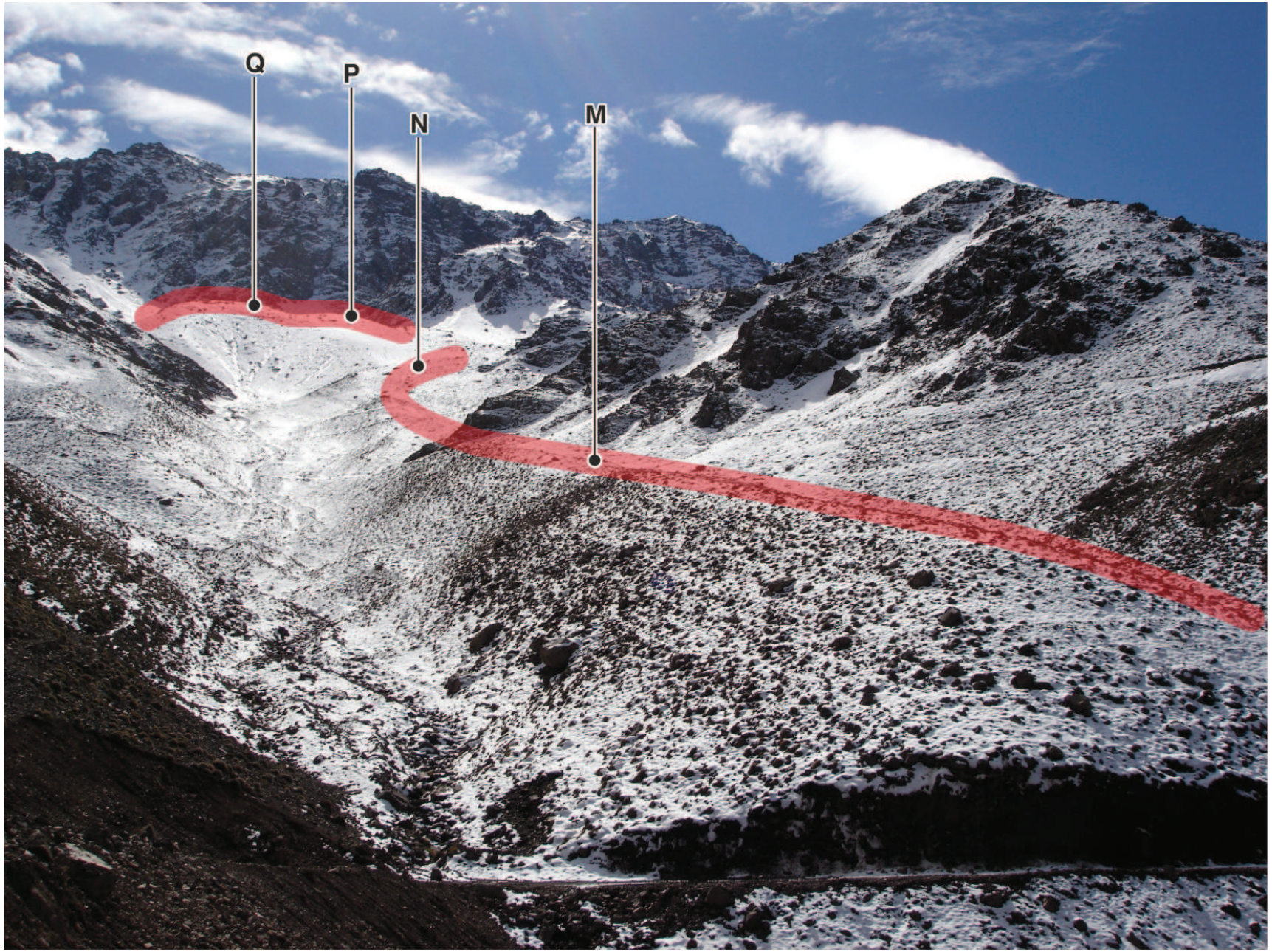
Q
P
N
M


Truncated spur
Toubkal-1; AD
Perched boulder

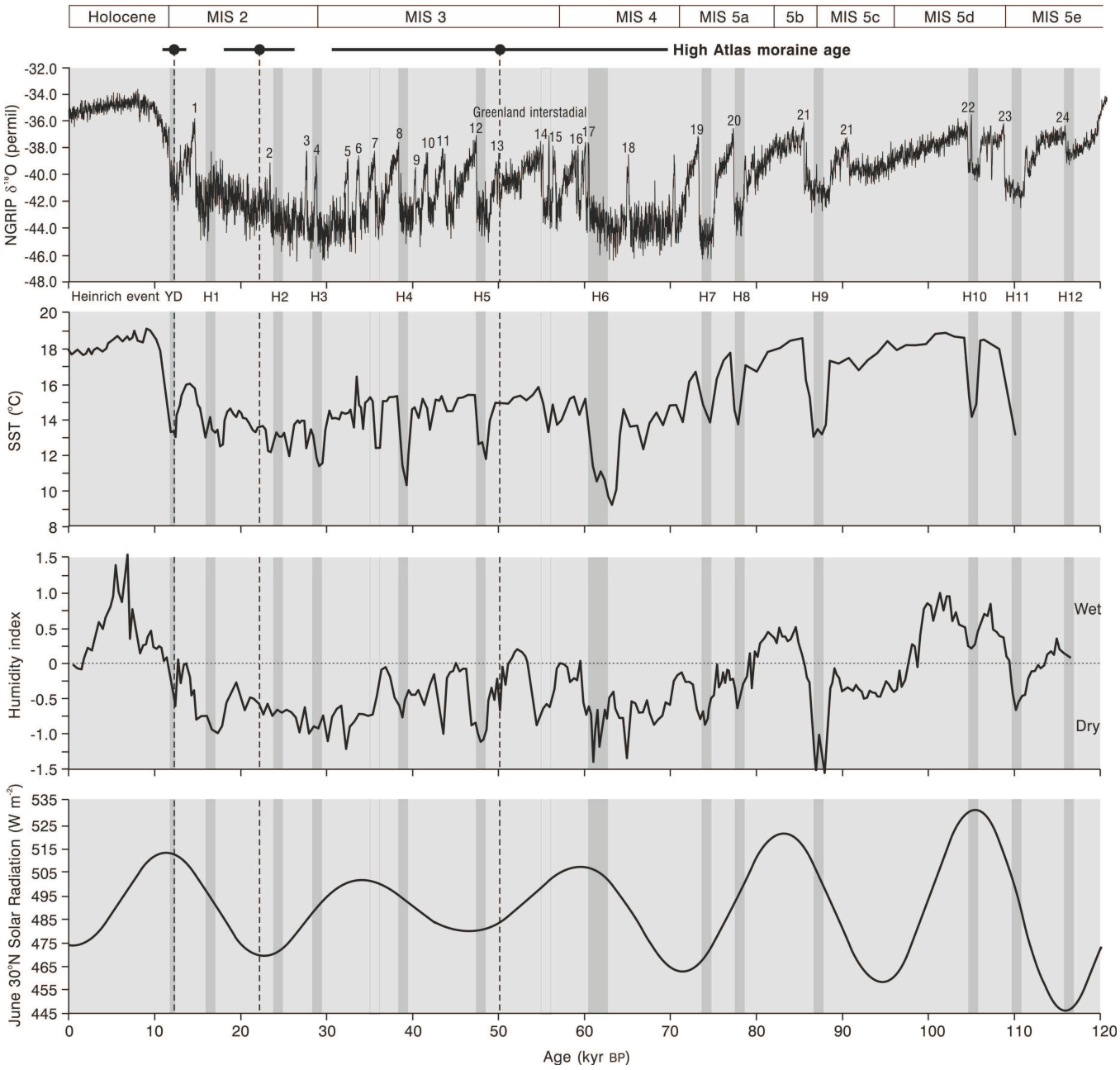
Holocene
MIS 2
MIS 3
MIS 4
MIS 5a
5b
MIS 5c
MIS 5d
MIS 5e
High Atlas moraine age
NGRIP δ18O (permil)
Greenland interstadial
Heinrich event
YD
H1
H2
H3
H4
H5
H6
H7
H8
H9
H10
H11
H12
SST (°C)
Humidity index
Wet
Dry
June 30°N Solar Radiation (W m-2)
Age (kyr BP)

**Table 1.** Valley morphometry data for the nine glaciated valleys in this study.

| Mountain area | Valley | Lowest moraine altitude (m) | Upper catchment elevation (m) | Glaciated valley length (km) | Glaciated valley max width (km) |
|---|---|---|---|---|---|
| Aksoual-Bou Iguenouane | Amguedoul | 2350 | 3625 | 2.5 | 0.8 |
| Aksoual-Bou Iguenouane | Iguenouane | 2150 | 3800 | 4.2 | 1.5 |
| Aksoual-Bou Iguenouane | Likemt | 2100 | 3550 | 3.1 | 1.8 |
| Aksoual-Bou Iguenouane | Goudmane | 2180 | 3800 | 3.9 | 1.5 |
| Aksoual-Bou Iguenouane | Tamda | 2080 | 3300 | 2.75 | 0.8 |
| Aksoual-Bou Iguenouane | Tamatert | 1880 | 3300 | 3.75 | 0.8 |
| Aksoual-Bou Iguenouane | Imserdane | <1700 | 3700 | >4.5 | 1.5 |
| Adrar el Hajj | Mzik | 1950 | 3000 | 2.0 | 1.0 |
| Toubkal | Mizane | 1900 | 4100 | 9.0 | 2.0 |

**TABLE 2. Sample site data (all samples).**

| Alphabetic label | Region | Sample name | SUERC-ANSTO | 36Cl or 10Be | Elevation | Latitude | Longitude | Thickness | Density | Topographic shielding | Boulder size |
|---|---|---|---|---|---|---|---|---|---|---|---|
| | | | | | (m) | (N) | (W) | (cm) | (g/cm3) | | (H xL x W) m |
| A | Aksoual/ | AT-4 | SUERC | 36Cl | 2220 | 31.1376 | -7.8935 | 5 | 2.8 | 0.960 | 1.5x2x1.5 |
| B | Imenane valley | AT-3a $ | SUERC | 36Cl | 2220 | 31.1376 | -7.8935 | 5 | 2.8 | 0.960 | 1.75x2x2 |
| C | (see Figure 3 - Region 1) | IT-10 | SUERC | 36Cl | 2238 | 31.1491 | -7.8618 | 1 | 2.7 | 0.982 | 4x8x6 |
| D | | TAM-7 | ANSTO | 10Be | 2144 | 31.1528 | -7.8624 | 4 | 2.7 | 0.990 | 3x4x3 |
| E | | TAM-2 | SUERC | 10Be | 2154 | 31.1526 | -7.8623 | 5 | 3.4 | 0.920 | 1.25x1.5x1.5 |
| F | | TAM-5 # | SUERC | 36Cl | 2265 | 31.1492 | -7.8583 | 5 | 2.8 | 0.986 | 1.25x1.25x1.25 |
| G | | TAM-4 | SUERC | 36Cl | 2380 | 31.1451 | -7.8583 | 5 | 2.8 | 0.986 | 0.75x0.75x0.75 |
| G | | TAM-6 | SUERC | 36Cl | 2380 | 31.1451 | -7.8583 | 3 | 3.4 | 0.986 | 1x1.5x1.5 |
| H | | Irhzwe-10-11 | ANSTO | 10Be | 2274 | 31.1518 | -7.8507 | 3 | 2.7 | 0.945 | 1.5x2x1.5 |
| J | | Irhzwe-9-11 | ANSTO | 10Be | 2309 | 31.1515 | -7.8493 | 5 | 2.7 | 0.950 | 1.5x2x1.5 |
| K | | Irhzwe-12-11 | SUERC | 36Cl | 2392 | 31.1501 | -7.8443 | 5 | 2.8 | 0.981 | 2x2.5x2.5 |
| L | | Irhzwe-6-10 # | SUERC | 36Cl | 2594 | 31.1439 | -7.8420 | 5 | 2.8 | 0.937 | 0.75x0.75x0.75 |
| L | | Irhzwe-7-10 | ANSTO | 10Be | 2583 | 31.1442 | -7.8442 | 3 | 2.7 | 0.937 | 1x1x1 |
| L | | Irhzwe-2-10 | ANSTO | 10Be | 2576 | 31.1443 | -7.8422 | 3 | 2.7 | 0.937 | 0.5x0.5x0.5 |
| M | | Irhzwe-4-10 | SUERC | 36Cl | 2568 | 31.1445 | -7.8434 | 5 | 2.8 | 0.940 | 2.5x4x3 |
| M | | Irhzwe-5-10 | ANSTO | 10Be | 2553 | 31.1447 | -7.8434 | 6 | 2.7 | 0.961 | 0.5x0.5x0.5 |
| N | | Irhzwe-3-10 | SUERC | 36Cl | 2940 | 31.1362 | -7.8414 | 5 | 2.8 | 0.989 | 1.5x1.5x1.5 |
| P | | Irhwze-1 | SUERC | 10Be | 2975 | 31.1359 | -7.8400 | 1 | 2.7 | 0.991 | 3x4x3.5 |
| Q | | Irhzwe-8-10 | ANSTO | 10Be | 3035 | 31.1351 | -7.8405 | 1 | 2.7 | 0.991 | 1.5x1.5x1.5 |
| R | | Amguedoul-1 | SUERC | 36Cl | 2440 | 31.1553 | -7.8363 | 5 | 2.8 | 0.976 | 1.5x1.5x1.25 |
| R | | Amguedoul-7 | ANSTO | 10Be | 2395 | 31.1552 | -7.8377 | 2 | 2.7 | 0.961 | 1x1.25x1 |
| S | | Amguedoul-2 | SUERC | 10Be | 2460 | 31.1554 | -7.8359 | 5 | 2.7 | 0.961 | 1.75x1.75x1.5 |
| T | | Amguedoul-3 | ANSTO | 10Be | 2475 | 31.1578 | -7.8346 | 2 | 2.7 | 0.950 | 2.5x2.5x2.5 |
| U | | Amguedoul-6 | ANSTO | 10Be | 2500 | 31.1571 | -7.8330 | 2 | 2.7 | 0.988 | 2x2x1.5 |
| AG | | A-12 | SUERC | 36Cl | 2210 | 31.1261 | -7.9025 | 5 | 2.8 | 0.925 | 1.5x1.75x1.75 |
| AH | | A-14 | SUERC | 36Cl | 2210 | 31.1258 | -7.9021 | 5 | 2.8 | 0.925 | 2.75x3x2.75 |
| V | Adrar el Hajj | AM-11-11 | SUERC | 36Cl | 2012 | 31.1312 | -7.9360 | 5 | 2.8 | 0.981 | 1.75x2x1.75 |
| W | (See Figure 4 - Region 2) | AM-2 | SUERC | 10Be | 2063 | 31.1297 | -7.9338 | 1 | 2.7 | 0.972 | 1x0.75x0.75 |
| W | | AM-3 | SUERC | 10Be | 2063 | 31.1296 | -7.9338 | 2 | 2.7 | 0.942 | 0.75x1x0.75 |
| X | | AM-7 | SUERC | 10Be | 2125 | 31.1283 | -7.9411 | 2 | 2.8 | 0.965 | 1.5x2x1.75 |
| X | | AM-10-11 | ANSTO | 10Be | 2124 | 31.1284 | -7.9410 | 10xx | 2.7 | 0.945 | 0.5x1x1 |
| X | | AM-8-11 | SUERC | 36Cl | 2112 | 31.1287 | -7.9409 | 5 | 2.8 | 0.972 | 0.75x1.25x0.5 |
| Y | | AM-9-11 | SUERC | 36Cl | 2133 | 31.1282 | -7.9411 | 5 | 2.8 | 0.991 | 1.5x2x1.5 |
| Y | | IGL-7 | SUERC | 10Be | 2080 | 31.1283 | -7.9396 | 5 | 3.4 | 0.941 | 1x1.5x1.5 |
| Z | | AM-4 * | SUERC | 10Be | 2023 | 31.1308 | -7.9365 | 1 | 2.7 | 0.913 | Bedrock |
| Z | | IGL-10 | SUERC | 10Be | 2114 | 31.128 | -7.9390 | 5 | 2.5 | 0.933 | 1.5x1.5x1.5 |
| AA | Ait Mizane/Toubkal | Toubkal-4 | SUERC | 36Cl | 2010 | 31.1120 | -7.9210 | 1 | 2.7 | 0.965 | 2.5x2.5x2.5 |
| AB | (See Figure 5 - Region 3) | Toubkal-3 | SUERC | 36Cl | 2080 | 31.1120 | -7.9204 | 1 | 2.7 | 0.968 | 1x1.5x1.5 |
| AC | | Toubkal-2 * | SUERC | 10Be | 2268 | 31.1017 | -7.9163 | 5 | 2.7 | 0.899 | Bedrock |

| | | | | | | | | | | |
|---|---|---|---|---|---|---|---|---|---|---|
| AD | Toubkal-1 * | ANSTO | 10Be | 2271 | 31.1017 | -7.9162 | 1 | 2.7 | 0.982 | Bedrock |
| AE | TT-1 * | SUERC | 10Be | 2570 | 31.0966 | -7.9060 | 1 | 2.7 | 0.896 | Bedrock |
| AF | SC-1 | SUERC | 10Be | 2510 | 31.0938 | -7.9148 | 5 | 2.7 | 0.900 | 0.5x0.5x0.5 |

* bedrock sample

# duplicate sample processed from same grain size (125-250 um)

$ duplicate sample processed from two separte grain size fractions 125-250 and 250-500 um

xx Thin (~1 cm) quartz vein sampled up to 10 cm into boulder in order to obtain sufficient mass

**TABLE 3. 10Be isotope data.**

| Lab | Alphabetic label | Region | Sample name | $^{10}Be/^{9}Be$ | $^{10}Be/^{9}Be$ error (a) | Quartz mass | $^{9}Be$ spike mass | $^{10}Be$ conc. | $^{10}Be$ conc. Error (b) |
|---|---|---|---|---|---|---|---|---|---|
| | | | | (NIST_27900) x 1E-15 | (%) | (g) | (mg) | (atoms/gram) x 1E3 | (atoms/gram) x 1E3 |
| ansto | D | Aksoual/ Imenane valley (see Figure 3 - Region 1) | TAM-7 | 195.2 | 2.8 | 11.823 | 0.320 | 357.4 | 12.9 |
| suerc | E | | TAM-2 | 226.3 | 5.1 | 15.017 | 0.232 | 233.6 | 5.7 |
| ansto | H | | Irhzwe-10-11 | 109.5 | 3.9 | 12.714 | 0.380 | 218.6 | 9.8 |
| ansto | J | | Irhzwe-9-11 | 470.2 | 2.5 | 19.695 | 0.380 | 605.7 | 20.2 |
| ansto | L | | Irhzwe-7-10 | 126.3 | 7.1 | 26.100 | 0.379 | 122.7 | 9.1 |
| ansto | L | | Irhzwe-2-10 | 367.5 | 3.0 | 17.989 | 0.380 | 519.3 | 19.2 |
| ansto | M | | Irhzwe-5-10 | 162.2 | 2.5 | 26.011 | 0.380 | 158.5 | 5.3 |
| suerc | P | | Irhzwe-1 | 119.3 | 5.6 | 5.004 | 0.200 | 318.6 | 15.3 |
| ansto | Q | | Irhzwe-8-10 | 113.5 | 3.0 | 7.674 | 0.379 | 374.6 | 14.1 |
| suerc | S | | Ameguedoul-2 | 835.6 | 13.2 | 6.548 | 0.204 | 1739.5 | 32.5 |
| ansto | R | | Amguedoul-7 | 112.0 | 2.7 | 10.718 | 0.322 | 225.1 | 7.8 |
| ansto | T | | Amguedoul-3 | 182.6 | 2.6 | 23.023 | 0.322 | 170.7 | 5.9 |
| ansto | U | | Amguedoul-6 | 45.0 | 4.8 | 3.464 | 0.215 | 186.7 | 9.9 |
| suerc | W | Adrar el Hajj (See Figure 4 - Region 2) | AM-2 | 261.1 | 7.0 | 3.652 | 0.152 | 726.3 | 20.8 |
| suerc | W | | AM-3 | 321.4 | 8.1 | 9.442 | 0.222 | 505.0 | 13.7 |
| suerc | X | | AM-7 | 302.7 | 7.6 | 11.721 | 0.230 | 396.9 | 10.7 |
| ansto | X | | AM-10-11 | 475.8 | 1.4 | 46.360 | 0.380 | 260.6 | 6.9 |
| suerc | Y | | IGL-7 | 59.4 | 2.0 | 5.003 | 0.201 | 159.5 | 5.7 |
| suerc | Z | | AM-4 | 84.8 | 3.5 | 7.994 | 0.219 | 155.3 | 6.5 |
| suerc | Z | | IGL-10 | 66.1 | 2.6 | 5.004 | 0.201 | 177.5 | 7.1 |
| *suerc* | AC | (See Figure 5 - Region 3) Ait Mizane/Toubkal | Toubkal-2 | 289.6 | 7.3 | 10.787 | 0.2486 | 446.0 | 12.1 |
| *ansto* | AD | | Toubkal-1 | 643.8 | 2.6 | 14.214 | 0.320 | 981.6 | 34.0 |
| *suerc* | AE | | TT-1 | 191.7 | 5.3 | 14.605 | 0.2499 | 219.1 | 6.5 |
| *suerc* | AF | | SC-1 | 121.4 | 3.4 | 14.003 | 0.2197 | 127.2 | 3.7790 |

**All samples** normalised to NIST-SRM-4325 with with a 10Be/9Be value of 27,900E-15.

(a) Final AMS $^{10}Be/^{9}Be$ ratio from weighted mean of repeat measurements. All AMS ratios corrected for full chemistry procedural blank

(b) Total analytical error in 10Be concentration based on final AMS 10Be/9Be error, 1% error in 9Be spike value and a 1 or 2% reproducibility error based on the standard deviation from long term repeat measure of the NIST-4325 primary standard.

**TABLE 4. 36Cl isotope and major element geochemistry data (see Supplementary Tables for full geochemistry data)**

| Alphabetic label | Region | Sample name | K2O | CaO | TiO2 | Fe2O3 | Cl (a) | sample mass | 36Cl/Cl (b) | 36Cl/Cl error | 36Cl concentration (atoms/gram) | 36Cl conc error |
|---|---|---|---|---|---|---|---|---|---|---|---|---|
| | | | wt% | wt% | wt% | wt% | ppm | g | x 1E-15 | x 1E-15 | | |
| A | Aksoual/ | AT-4 | 6.82 ± 1.02 | 0.35 ± 0.02 | 1.22 ± 0.18 | 15.61 ± 0.78 | 257 | 14.80 | 1059.80 | 20.79 | 4540867 | 85182 |
| B | Imenane valley | AT-3a (125-250 um) | 9.90±1.49 | 0.10±0.005 | 1.30±0.20 | 6.86±0.34 | 178 | 15.03 | 1131.10 | 30.24 | 3358089 | 82434 |
| B | (see Figure 3 - Region 1) | AT-3a (250-500 um) | 10.17±1.53 | 0.11±0.01 | 1.28±0.19 | 7.38±0.37 | 179 | 15.13 | 1061.90 | 22.52 | 3247893 | 70167 |
| C | | IT-10 | 2.28±0.01 | 0.30±0.001 | 1.34±0.01 | 5.70±0.05 | 279 | 15.60 | 236.84 | 5.21 | 1475073 | 70412 |
| F | | TAM-5 (125-250 um) | 3.95±0.59 | 5.36±0.27 | 1.42±0.21 | 14.53±0.73 | 210 | 14.96 | 1159.10 | 27.77 | 4184920 | 90617 |
| F | | TAM-5 (125-250 um) | 4.10±0.61 | 5.43±0.27 | 1.42±0.21 | 14.30±0.71 | 203 | 15.02 | 1086.10 | 29.97 | 3719658 | 89337 |
| G | | TAM-4 | 3.94±0.59 | 0.08±0.004 | 0.72±0.11 | 10.75±0.54 | 408 | 9.55 | 15.87 | 0.45 | 965265 | 54958 |
| G | | TAM-6 | 4.02±0.03 | 0.23±0.003 | 0.79±0.003 | 6.16±0.02 | 262 | 12.51 | 283.03 | 8.40 | 1796434 | 78145 |
| K | | Irhzwe-12-11 | 1.81±0.02 | 1.00±0.01 | 1.09±0.01 | 7.94±0.05 | 281 | 10.56 | 163.42 | 4.90 | 1142489 | 47841 |
| L | | Irhzwe-6-10 (125-250 um) | 6.12±0.92 | 0.20±0.01 | 1.15±0.17 | 18.10±0.91 | 391 | 15.18 | 158.47 | 3.95 | 1532373 | 30836 |
| L | | Irhzwe-6-10 (125-250 um) | 6.22±0.93 | 0.20±0.01 | 1.17±0.18 | 17.36±0.87 | 361 | 14.99 | 142.19 | 4.11 | 820763 | 21002 |
| M | | Irhzwe-4-10 | 5.73±0.86 | 0.62±0.03 | 1.02±0.15 | 18.27±0.91 | 363 | 15.00 | 195.11 | 5.59 | 1156672 | 27365 |
| N | | Irhzwe-3-10 | 2.83±0.02 | 0.19±0.002 | 0.58±0.00 | 5.32±0.04 | 239 | 10.85 | 237.21 | 5.22 | 1476170 | 49666 |
| R | | Amguedoul-1 | 6.12±0.92 | 0.60±0.03 | 0.67±0.10 | 14.18±0.71 | 522 | 20.50 | 97.06 | 2.65 | 9840853 | 890589 |
| AG | | A-12 | 6.46±0.97 | 1.01±0.05 | 1.10±0.17 | 17.79±0.89 | 226 | 9.86 | 51.81 | 0.27 | 306452 | 16752 |
| AH | | A-14 | 5.20±0.78 | 3.23±0.16 | 1.40±0.21 | 20.53±1.03 | 297 | 14.95 | 56.57 | 1.62 | 250251 | 8224 |
| V | Adrar el Hajj | AM-11-11 | 2.35±0.02 | 0.12±0.0008 | 0.24±0.001 | 5.03±0.02 | 171 | 16.98 | 64.48 | 1.92 | 274189 | 11395 |
| X | (See Figure 4 - Region 2) | AM-8-11 | 1.55±0.01 | 0.35±0.003 | 1.15±0.01 | 8.14±0.04 | 169 | 15.18 | 24.23 | 1.02 | 104257 | 5261 |
| Y | | AM-9-11 | 1.66±0.02 | 0.62±0.01 | 0.47±0.005 | 4.70±0.05 | 109 | 13.63 | 107.34 | 2.93 | 379953 | 12104 |
| AA | Ait Mizane/Toubkal | Toubkal-3 | 2.29±0.01 | 0.22±0.002 | 0.75±0.01 | 6.99±0.06 | 179 | 12.20 | 195.60 | 5.86 | 970933 | 36040 |
| AB | (See Figure 5 - Region 3) | Toubkal-4 | 5.19±0.04 | 0.90±0.01 | 1.02±0.01 | 7.57±0.08 | 429 | 15.28 | 413.72 | 11.36 | 3647500 | 284446 |

(a) Stable Cl concentrations were calculated by AMS isotope dilution (Di Nicola et al. 2009). All samples were spiked with c. 1.3 mg of non-natural Cl with a 35Cl/37Cl ratio of c. 20 atoms/atom.
(b) Standard Z93-0005 with a nominal 36Cl/Cl ratio of 1.2 E10-12 (PRIME Lab, Purdue University) was used as primary standard for 36Cl measurements
(c) Blank corrections for 36Cl concentrations ranged from between 0.5 and 25%
(d) repeat chemistry processing on same size fraction for L (Irhzwe-6) and F (TAM-5)
(e ) repeat chemistry processing on larger grain fraction (ie 250-500 um) for B (AT-3a)

**TABLE 5. Relative 36Cl production (see Supplementary Tables for full datasets)**

| Alphabetic label | Region | Sample name | Scaling Ca, K, Cl | Prod. from Ca (%) | Prod. from K (%) | Prod. from Cl (%) |
|---|---|---|---|---|---|---|
| A | Aksoual/ | AT-4 | 4.4662 | 0.7 | 47.0 | 51.0 |
| B | Imenane valley | AT-3a (125-250 um) | 4.4662 | 0.2 | 64.3 | 34.9 |
| B | (see Figure 3 - Region 1) | AT-3a (250-500 um) | 4.4662 | 0.2 | 64.7 | 34.4 |
| C | | IT-10 | 4.5188 | 1.0 | 25.4 | 72.6 |
| F | | TAM-4 | 4.9507 | 0.1 | 21.5 | 77.7 |
| F | | TAM-5 (125-250 um) | 4.5985 | 14.0 | 35.1 | 49.3 |
| F | | TAM-5 (125-250 um) | 4.5985 | 14.2 | 36.5 | 47.7 |
| G | | TAM-6 | 4.9507 | 0.6 | 34.2 | 64.6 |
| K | | Irhzwe-12-11 | 4.9887 | 2.7 | 16.8 | 79.5 |
| L | | Irhzwe-6-10 (125-250 um) | 5.6633 | 0.3 | 34.7 | 63.8 |
| L | | Irhzwe-6-10 (125-250 um) | 5.6633 | 0.3 | 36.8 | 61.7 |
| M | | Irhzwe-4-10 | 5.5727 | 1.1 | 33.7 | 64.1 |
| N | | Irhzwe-3-10 | 6.9845 | 0.5 | 26.7 | 72.2 |
| R | | Amguedoul-1 | 5.1435 | 0.9 | 29.9 | 68.5 |
| AG | | A-12 | 4.4362 | 2.2 | 48.2 | 48.1 |
| AH | | A-14 | 4.4361 | 6.5 | 35.2 | 56.7 |
| V | Adrar el Hajj | AM-11-11 | 3.8948 | 0.4 | 28.8 | 70.1 |
| X | (See Figure 4 - Region 2) | AM-8-11 | 4.1620 | 1.5 | 22.0 | 75.0 |
| Y | | AM-9-11 | 4.2200 | 3.2 | 28.8 | 67.0 |
| AA | Ait Mizane/Toubkal | Toubkal-4 | 4.0716 | 1.0 | 33.7 | 64.1 |
| AB | (See Figure 5 - Region 3) | Toubkal-3 | 3.8869 | 1.7 | 33.9 | 63.7 |

**TABLE 6. Glacial phases showing 10Be and 36Cl ages grouped by stratigraphical unit (3 = youngest and highest moraines, 1 = oldest and lowest moraines)**

| Glacial Stratigraphical Unit | Region | Alphabetic label | Sample ID | 10Be age | Age error | 36Cl age | Age error (a) |
|---|---|---|---|---|---|---|---|
| | | | | ka | ka | ka | ka |
| **Glacial UNIT-3** | **Region 1** | Q | Irhzwe-8-10 | 13.7 | 0.8 | | |
| | | P | Irhzwe-1 | 12.1 | 0.8 | | |
| | **Region 2** | Y | IGL-10 | 12.5 | 0.8 | | |
| | | Y | AM-4 | 11.5 | 0.7 | | |
| | | Z | IGL-7 | 11.5 | 0.7 | | |
| | | X | AM-9-11 | | | 13.2 | 0.7 |
| | **Region 3** | AE | TT-1 | 11.7 | 0.7 | | |
| | | | Mean Age (n=7) | 12.3 | St Dev | 0.9 | |
| | | | | No Outliers | | | |
| | | | | | | | |
| **Glacial UNIT-2** | **Region 1** | C | IT-10 | | | 29.5 | 1.7 |
| | | D | TAM-7 | 22.5 | 1.4 | | |
| | | E | TAM-2 | 16.3 | 0.9 | | |
| | | G | TAM-6 | | | 26.1 | 1.3 |
| | | K | Irhzwe-12-11 | | | 17.2 | 0.9 |
| | | L | Irhzwe-2-10 | 25.8 | 1.6 | | |
| | | N | Irhzwe-3 | | | 16.6 | 0.8 |
| | **Region 2** | X | AM-10-11 | 18.6 | 1.0 | | |
| | | X | AM-7 | 25.3 | 1.4 | | |
| | | | Mean Age (n=9) | 22.0 | St Dev | 4.9 | |
| | | | | Outliers (n=7) | | | |
| | | *L ** | *Irhzwe-6** | | | *9.0* | *4.5* |
| | | *L* | *Irhzwe-7-10* | *6.3* | *0.6* | | |
| | | *M* | *Irhzwe-4* | | | *8.9* | *0.6* |
| | | *M* | *Irhzwe-5-10* | *8.2* | *0.5* | | |
| | | *X* | *AM-8-11* | | | *2.7* | *0.9* |
| | | *AG* | *A-12* | | | *4.4* | *0.9* |
| | | *AH* | *A-14* | | | *1.1* | *0.2* |
| | | | | | | | |
| **Glacial UNIT-1** | **Region 1** | A | AT-4 | | | 60.0 | 4.7 |
| | | B * | AT-3a* | | | 39.5 | 5.0 |
| | | F * | TAM-5* | | | 63.3 | 5.8 |
| | | H | Irhzwe-9-11 | 34.6 | 2.0 | | |
| | | R | Amguedoul-1 | | | 80.0 | 12.1 |
| | | S | Amguedoul-2 | 87.9 | 4.7 | | |
| | **Region 2** | W | AM2 | 44.2 | 2.6 | | |
| | | W | AM3 | 33.4 | 1.9 | | |
| | **Region 3** | AA | Toubkal-4 | | | 50.0 | 4.9 |
| | | AB | Toubkal-3 | | | 28.9 | 1.4 |
| | | AC | Toubkal-2 | 28.2 | 1.5 | | |
| | | AD | Toubkal-1 | 52.0 | 3.1 | | |
| | | | Mean Age (n=12) | 50.2 | St Dev | 19.5 | |
| | | | | Outliers (n=7) | | | |
| | | *G* | *TAM-4* | | | *6.0* | *0.4* |
| | | *J* | *Irhzwe-10-11* | *13.6* | *0.9* | | |
| | | *R* | *AMGUEDOUL-7* | *12.6* | *0.8* | | |
| | | *T* | *AMGUEDOUL-3* | *9.1* | *0.5* | | |
| | | *U* | *AMGUEDOUL-6* | *9.5* | *0.7* | | |
| | | *V* | *AM-11-11* | | | *7.2* | *0.6* |
| | | *AF* | *SC-1* | *7.1* | *0.4* | | |

* Multiple ages from the same sample. The average is used to calculate the overall mean and standard deviation for the group
(a) Internal analytical errors. Total errors for 36Cl can be seen in Supplementary Table 3
All ages are calculated in Cronus using the North East North America (NENA) production rates: http://hess.ess.washington.edu/math/al_be_v22/alt_cal/Balco_NENA_age_input.html
Ages are reported using the Lal (1991)/Stone (1990) time-dependent scaling sheme (Lm)

**Supplementary Files**

**Supplementary Table 1.** Raw CRONUS inputs for 10Be calculation.
http://hess.ess.washington.edu/math/al_be_v22/alt_cal/Balco_NENA_age_input.html

| Sample name | Lat N | Long E | Alt m | | Thickness | Density | Shielding | Erosion | 10Be/g | 10Be/g error | Standardization | 26Al/g | 26Al/g error | Standardization |
|---|---|---|---|---|---|---|---|---|---|---|---|---|---|---|
| TAM7 | 31.1528 | -7.8624 | 2144 | std | 4 | 2.7 | 0.99 | 0 | 357356 | 12854 | NIST_27900 | 0 | 0 | KNSTD |
| TAM2 | 31.1526 | -7.8623 | 2154 | std | 5 | 3.4 | 0.92 | 0 | 233583 | 5715 | NIST_27900 | 0 | 0 | KNSTD |
| Irhzwe-10-11 | 31.1518 | -7.8507 | 2274 | std | 3 | 2.7 | 0.945 | 0 | 218600 | 9800 | NIST_27900 | 0 | 0 | KNSTD |
| Irhzwe-9-11 | 31.1515 | -7.8493 | 2309 | std | 5 | 2.7 | 0.95 | 0 | 605700 | 20200 | NIST_27900 | 0 | 0 | KNSTD |
| Irhzwe-7-10 | 31.1442 | -7.8422 | 2583 | std | 3 | 2.7 | 0.937 | 0 | 122700 | 9100 | NIST_27900 | 0 | 0 | KNSTD |
| Irhzwe-2-10 | 31.1443 | -7.8422 | 2576 | std | 3 | 2.7 | 0.937 | 0 | 519300 | 19200 | NIST_27900 | 0 | 0 | KNSTD |
| Irhzwe-5-10 | 31.1447 | -7.8434 | 2553 | std | 6 | 2.7 | 0.961 | 0 | 158500 | 5300 | NIST_27900 | 0 | 0 | KNSTD |
| IRHZWE-1 | 31.1359 | -7.8400 | 2975 | std | 1 | 2.7 | 0.991 | 0 | 318614 | 15282 | NIST_27900 | 0 | 0 | KNSTD |
| Irhzwe-8-10 | 31.1351 | -7.8405 | 3035 | std | 1 | 2.7 | 0.991 | 0 | 374763 | 14066 | NIST_27900 | 0 | 0 | KNSTD |
| AMGUEDOUL-7 | 31.1552 | -7.8377 | 2395 | std | 2 | 2.7 | 0.961 | 0 | 225068 | 7822 | NIST_27900 | 0 | 0 | KNSTD |
| AMGUEDOUL-2 | 31.1554 | -7.8359 | 2460 | std | 5 | 2.7 | 0.961 | 0 | 1739536 | 32473 | NIST_27900 | 0 | 0 | KNSTD |
| AMGUEDOUL-3 | 31.1578 | -7.8346 | 2475 | std | 2 | 2.7 | 0.95 | 0 | 170711 | 5877 | NIST_27900 | 0 | 0 | KNSTD |
| AMGUEDOUL-6 | 31.1571 | -7.8330 | 2500 | std | 2 | 2.7 | 0.988 | 0 | 186654 | 9925 | NIST_27900 | 0 | 0 | KNSTD |
| AM-2 | 31.1297 | -7.9338 | 2063 | std | 1 | 2.7 | 0.972 | 0 | 726279 | 20844 | NIST_27900 | 0 | 0 | KNSTD |
| AM-3 | 31.1296 | -7.9338 | 2063 | std | 2 | 2.7 | 0.942 | 0 | 504959 | 13741 | NIST_27900 | 0 | 0 | KNSTD |
| AM-7 | 31.1283 | -7.9411 | 2125 | std | 2 | 2.8 | 0.965 | 0 | 396924 | 10670 | NIST_27900 | 0 | 0 | KNSTD |
| AM-10-11 | 31.1284 | -7.9410 | 2124 | std | 10 | 2.7 | 0.941 | 0 | 260600 | 6900 | NIST_27900 | 0 | 0 | KNSTD |
| IGL-7 | 31.1283 | -7.9396 | 2080 | std | 5 | 3.4 | 0.941 | 0 | 159537 | 5681 | NIST_27900 | 0 | 0 | KNSTD |
| AM-4 | 31.1308 | -7.9365 | 2023 | std | 1 | 2.7 | 0.913 | 0 | 155263 | 6505 | NIST_27900 | 0 | 0 | KNSTD |
| IGL-10 | 31.128 | -7.9390 | 2114 | std | 5 | 2.5 | 0.933 | 0 | 177477 | 7129 | NIST_27900 | 0 | 0 | KNSTD |
| TOUBKAL-1 | 31.1017 | -7.9162 | 2271 | std | 1 | 2.7 | 0.982 | 0 | 981597 | 33965 | NIST_27900 | 0 | 0 | KNSTD |
| TOUBKAL-2 | 31.1017 | -7.9163 | 2268 | std | 5 | 2.7 | 0.899 | 0 | 445977 | 12059 | NIST_27900 | 0 | 0 | KNSTD |
| TT-1 | 31.0966 | 7.9060 | 2570 | std | 1 | 2.7 | 0.896 | 0 | 219147 | 6476 | NIST_27900 | 0 | 0 | KNSTD |
| SC-1 | 31.0938 | -7.9148 | 2510 | std | 5 | 2.7 | 0.9 | 0 | 127237 | 3779 | NIST_27900 | 0 | 0 | KNSTD |

**Supplementary Table 2. Raw CRONUS inputs for 36Cl calculation.**

http://cronus.cosmogenicnuclides.rocks/2.0/html/cl/

| Sample Name | Scaling | Latitude | Longitude | Elevation | Pressure (calculated from elevation) | Atmospheric Pressure or Elevation | Sample Thickness | Bulk Density | Shielding Factor | Erosion Rate | Conc. 36Cl | Attenuation length | Depth to Top of Sample | Year Collected | Water Content in Pores | Mineral Separation |
|---|---|---|---|---|---|---|---|---|---|---|---|---|---|---|---|---|
| AT-4125-250m | LM | 31.1376 | -7.8935 | 2220 | 782.5098 | Elevation | 5 | 2.8 | 0.96 | 0 | 4540867 | 177 | 0 | 2000 | 0.01 | Yes |
| AT-3a1125-250 | LM | 31.1376 | -7.8935 | 2220 | 782.5098 | Elevation | 5 | 2.8 | 0.96 | 0 | 3358089 | 177 | 0 | 2000 | 0.01 | Yes |
| AT-3a2250-500 | LM | 31.1376 | -7.8935 | 2220 | 782.5098 | Elevation | 5 | 2.8 | 0.96 | 0 | 3247893 | 177 | 0 | 2000 | 0.01 | Yes |
| IT-10 | LM | 31.1491 | -7.8618 | 2238 | 780.8315 | Elevation | 1 | 2.65 | 0.9823 | 0 | 1475073 | 177 | 0 | 2000 | 0.01 | No |
| TAM-4 | LM | 31.1451 | -7.8583 | 2380 | 767.5267 | Elevation | 5 | 2.8 | 0.9861 | 0 | 965265 | 177 | 0 | 2000 | 0.01 | Yes |
| TAM-51125-25( | LM | 31.1492 | -7.8583 | 2265 | 778.2894 | Elevation | 5 | 2.8 | 0.986 | 0 | 4184920 | 177 | 0 | 2000 | 0.01 | Yes |
| TAM-52125-25( | LM | 31.1492 | -7.8583 | 2265 | 778.2894 | Elevation | 5 | 2.8 | 0.986 | 0 | 3719658 | 177 | 0 | 2000 | 0.01 | Yes |
| TAM-6 | LM | 31.1451 | -7.8583 | 2380 | 767.5267 | Elevation | 3 | 3.41 | 0.986 | 0 | 1796434 | 177 | 0 | 2000 | 0.01 | No |
| IRHZWE-12-11 | LM | 31.1501 | -7.8443 | 2392 | 766.4209 | Elevation | 5 | 2.81 | 0.9813 | 0 | 1142489 | 177 | 0 | 2000 | 0.01 | No |
| IRHZWE-61125 | LM | 31.1439 | -7.842 | 2594 | 747.8365 | Elevation | 5 | 2.8 | 0.9368 | 0 | 1532373 | 177 | 0 | 2000 | 0.01 | Yes |
| IRHZWE-62125 | LM | 31.1439 | -7.842 | 2594 | 747.8365 | Elevation | 5 | 2.8 | 0.9368 | 0 | 820763 | 177 | 0 | 2000 | 0.01 | Yes |
| IRHZWE-4125-2 | LM | 31.1445 | -7.8434 | 2568 | 750.2065 | Elevation | 5 | 2.8 | 0.9401 | 0 | 1156672 | 177 | 0 | 2000 | 0.01 | Yes |
| IRHZWE-3 | LM | 31.1362 | -7.8414 | 2940 | 716.8571 | Elevation | 5 | 2.81 | 0.9885 | 0 | 1476170 | 177 | 0 | 2000 | 0.01 | No |
| AMEGUEDOUL | LM | 31.1553 | -7.8363 | 2440 | 761.9729 | Elevation | 5 | 2.8 | 0.9759 | 0 | 9840853 | 177 | 0 | 2000 | 0.01 | Yes |
| A-12 | LM | 31.1261 | -7.9025 | 2210 | 783.4561 | Elevation | 5 | 2.8 | 0.9251 | 0 | 306452 | 177 | 0 | 2000 | 0.01 | Yes |
| A-14125-250m | LM | 31.1258 | -7.9021 | 2210 | 783.4567 | Elevation | 5 | 2.8 | 0.9251 | 0 | 250251 | 177 | 0 | 2000 | 0.01 | Yes |
| AM-11-11 | LM | 31.1312 | -7.936 | 2012 | 802.3519 | Elevation | 5 | 2.8 | 0.9812 | 0 | 274189 | 177 | 0 | 2000 | 0.01 | No |
| AM-8-11 | LM | 31.1287 | -7.9409 | 2112 | 792.7408 | Elevation | 5 | 2.8 | 0.9723 | 0 | 104257 | 177 | 0 | 2000 | 0.01 | No |
| AM-9-11 | LM | 31.1282 | -7.9411 | 2133 | 790.7352 | Elevation | 5 | 2.8 | 0.9907 | 0 | 379953 | 177 | 0 | 2000 | 0.01 | No |
| TOUBKAL-3 | LM | 31.1083 | -7.9204 | 2080 | 795.8385 | Elevation | 1 | 2.65 | 0.965 | 0 | 970933 | 177 | 0 | 2000 | 0.01 | No |
| TOUBKAL-4 | LM | 31.112 | -7.921 | 2010 | 802.5712 | Elevation | 1 | 2.65 | 0.9682 | 0 | 3647500 | 177 | 0 | 2000 | 0.01 | No |

| Bulk Rock SiO2 | Bulk Rock TiO2 | Bulk Rock Al2O3 | Bulk Rock Fe2O3 | Bulk Rock MnO | Bulk Rock MgO | Bulk Rock CaO | Bulk Rock Na2O | Bulk Rock K2O | Bulk Rock P2O5 | Analytical Water | Bulk Rock CO2 | Bulk Rock Cl | Bulk Rock B |
|---|---|---|---|---|---|---|---|---|---|---|---|---|---|
| 52.31 | 1.218000585 | 19.059 | 11.203 | 0 | 5.806 | 2.089 | 4.218 | 3.346 | 0.418 | 1 | 1 | 257 | 0 |
| 60.363 | 1.301425283 | 16.5 | 8.379 | 0 | 2.541 | 1.091 | 4.22 | 4.651 | 1.005 | 1 | 1 | 178 | 0 |
| 60.363 | 1.284740343 | 16.5 | 8.379 | 0 | 2.541 | 1.091 | 4.22 | 4.651 | 1.005 | 1 | 1 | 179 | 0 |
| 63.2375278 | 1.335428385 | 16.71966609 | 5.704191824 | 0.018593673 | 0.347077123 | 0.298586402 | 10 | 2.28068041 | 0 | 1 | 1 | 278.6316249 | 0 |
| 67.417 | 0.585641377 | 16.339 | 4.637 | 0.125248999 | 0.231 | 0.901 | 6.119 | 2.673 | 0.534 | 1 | 1 | 408.0224383 | 0 |
| 47.001 | 1.418219859 | 17.462 | 13.047 | 0 | 9.648 | 6.036 | 3.24 | 1.49 | 0.707 | 1 | 1 | 210 | 0 |
| 47.001 | 1.418219859 | 17.462 | 13.047 | 0 | 9.648 | 6.036 | 3.24 | 1.49 | 0.707 | 1 | 1 | 203 | 0 |
| 66.3671911 | 0.786478245 | 15.26251249 | 6.156272295 | 0.023629459 | 0.490683807 | 0.225968622 | 6.613538728 | 4.019769993 | 0 | 1 | 1 | 262.0713052 | 0 |
| 62.7644318 | 1.086224037 | 14.39883911 | 7.938144183 | 0.064044873 | 0.931785167 | 0.997200228 | 10 | 1.805704291 | 0 | 1 | 1 | 281.1207492 | 0 |
| 51.753 | 1.151260827 | 17.663 | 10.848 | 0 | 6.306 | 3.684 | 5.121 | 2.514 | 0.697 | 1 | 1 | 391 | 0 |
| 51.753 | 1.167945766 | 17.663 | 10.848 | 0 | 6.306 | 3.684 | 5.121 | 2.514 | 0.697 | 1 | 1 | 361 | 0 |
| 53.695 | 1.017781311 | 16.606 | 10.837 | 0 | 6.078 | 3.007 | 5.229 | 2.279 | 0.652 | 1 | 1 | 363 | 0 |
| 67.389531 | 0.583478452 | 13.39647918 | 5.323883774 | 0.019626655 | 0.237796748 | 0.192388146 | 10 | 2.826487357 | 0 | 1 | 1 | 238.5247107 | 0 |
| 52.985 | 1.293082813 | 16.349 | 11.269 | 0.247915544 | 8.294 | 1.889 | 4.276 | 2.389 | 1.23 | 1 | 1 | 522.1879136 | 0 |
| 50.561 | 1.421556847 | 17.414 | 11.458 | 0.219508555 | 7.747 | 3.886 | 4.542 | 2.638 | 0.434 | 1 | 1 | 226.2579861 | 0 |
| 45.345 | 1.40153492 | 17.462 | 14.578 | 0 | 9.395 | 5.484 | 3.613 | 1.973 | 0.421 | 1 | 1 | 297 | 0 |
| 65.3821237 | 0.240030158 | 16.74441805 | 5.027214901 | 0.011621045 | 0.138963511 | 0.118930854 | 10 | 2.351270317 | 0 | 1 | 1 | 170.9359719 | 0 |
| 63.2075386 | 1.150443364 | 14.65788444 | 8.137305503 | 0.049195759 | 0.902765341 | 0.351475652 | 10 | 1.55370073 | 0 | 1 | 1 | 169.2530893 | 0 |
| 71.3270837 | 0.474055392 | 13.48660654 | 4.69866306 | 0.030731209 | 0.985844958 | 0.621238812 | 6.669075037 | 1.660790197 | 0 | 1 | 1 | 108.9066119 | 0 |
| 64.8454523 | 0.745110991 | 14.61537153 | 6.986087302 | 0.0227256 | 0.274610471 | 0.224849273 | 10 | 2.294171996 | 0 | 1 | 1 | 178.7458171 | 0 |
| 65.9935598 | 1.018668642 | 13.93610971 | 7.565556672 | 0.025953668 | 0.210766853 | 0.895899124 | 4.941653176 | 5.194381236 | 0 | 1 | 1 | 429.2779552 | 0 |

| Bulk Rock Sm | Bulk Rock Gd | Bulk Rock U | Bulk Rock Th | Bulk Rock Cr | Bulk Rock Li | Target K2O | Target CaO | Target TiO2 | Target Fe2O3 | Target Cl | Latitude Uncertainty | Longitude Uncertainty | Elevation Uncertainty |
|---|---|---|---|---|---|---|---|---|---|---|---|---|---|
| 0 | 0 | 8 | 5 | 120 | 0 | 6.818063189 | 0.349801637 | 1.218000585 | 15.61281354 | 257 | 0 | 0 | 10 |
| 0 | 0 | 8 | 5 | 60 | 0 | 9.901851487 | 0.097944458 | 1.301425283 | 6.862775181 | 178 | 0 | 0 | 10 |
| 0 | 0 | 8 | 5 | 60 | 0 | 10.16686454 | 0.111936524 | 1.284740343 | 7.37748332 | 179 | 0 | 0 | 10 |
| 4.685454678 | 4.359057138 | 1.326378051 | 1.148450505 | 0 | 0 | NaN | NaN | NaN | NaN | NaN | 0 | 0 | 10 |
| 0 | 0 | 9 | 5 | 0 | 0 | 3.939057708 | 0.083952393 | 0.717452399 | 10.75168112 | 408.0224383 | 0 | 0 | 10 |
| 0 | 0 | 8 | 5 | 330 | 0 | 3.951103756 | 5.358961076 | 1.418219859 | 14.52620747 | 210 | 0 | 0 | 10 |
| 0 | 0 | 8 | 5 | 330 | 0 | 4.095656333 | 5.428921403 | 1.418219859 | 14.29744829 | 203 | 0 | 0 | 10 |
| 3.680588065 | 2.635811656 | 0.810294126 | 0.925891958 | 0 | 0 | NaN | NaN | NaN | NaN | NaN | 0 | 0 | 10 |
| 2.556651691 | 2.624791312 | 3.478269138 | 4.587188902 | 0 | 0 | NaN | NaN | NaN | NaN | NaN | 0 | 0 | 10 |
| 0 | 0 | 8 | 5 | 140 | 0 | 6.119392403 | 0.195888917 | 1.151260827 | 18.10056954 | 391 | 0 | 0 | 10 |
| 0 | 0 | 8 | 5 | 140 | 0 | 6.215760788 | 0.195888917 | 1.167945766 | 17.35710223 | 361 | 0 | 0 | 10 |
| 0 | 0 | 8 | 5 | 90 | 0 | 5.733918866 | 0.615650881 | 1.017781311 | 18.27213892 | 363 | 0 | 0 | 10 |
| 3.014113738 | 2.652938964 | 3.726654767 | 4.827672209 | 0 | 0 | NaN | NaN | NaN | NaN | NaN | 0 | 0 | 10 |
| 0 | 0 | 8 | 4 | 220 | 0 | 6.119392403 | 0.601658815 | 0.667397581 | 14.18306871 | 522.1879136 | 0 | 0 | 10 |
| 0 | 0 | 2 | 2 | 90 | 0 | 6.456681748 | 1.007428714 | 1.101206008 | 17.78602568 | 226.2579861 | 0 | 0 | 10 |
| 0 | 0 | 8 | 5 | 110 | 0 | 5.203892752 | 3.232167124 | 1.40153492 | 20.53113575 | 297 | 0 | 0 | 10 |
| 3.328026533 | 2.058917496 | 0.522339239 | 0.698603969 | 0 | 0 | NaN | NaN | NaN | NaN | NaN | 0 | 0 | 10 |
| 1.522629088 | 1.404534111 | 0.949997877 | 1.337937815 | 0 | 0 | NaN | NaN | NaN | NaN | NaN | 0 | 0 | 10 |
| 2.405266447 | 2.168624414 | 1.707470158 | 2.094253098 | 0 | 0 | NaN | NaN | NaN | NaN | NaN | 0 | 0 | 10 |
| 2.549107883 | 2.336037475 | 1.151245983 | 1.57083224 | 0 | 0 | NaN | NaN | NaN | NaN | NaN | 0 | 0 | 10 |
| 3.598502092 | 3.448064819 | 0.934682157 | 1.082540811 | 0 | 0 | NaN | NaN | NaN | NaN | NaN | 0 | 0 | 10 |

| Pressure Uncertainty | Sample Thickness Uncertainty | Bulk Density Uncertainty | Shielding Factor Uncertainty | Erosion-Rate Uncertainty | Conc. 36Cl Uncertainty | Attenuation Length Uncertainty | Depth to Top of Sample Uncertainty | Year Collected Uncertainty | Water Content in Pores Uncertainty | Bulk Rock SiO2 Uncertainty | Bulk Rock TiO2 Uncertainty | Bulk Rock Al2O3 Uncertainty | Bulk Rock Fe2O3 Uncertainty |
|---|---|---|---|---|---|---|---|---|---|---|---|---|---|
| NaN | 0.5 | 0.2 | 0 | 0 | 85182 | 10 | 0 | 10 | 0.01 | 0.78465 | 0.018270009 | 0.285885 | 0.168045 |
| NaN | 0.5 | 0.2 | 0 | 0 | 82434 | 10 | 0 | 10 | 0.01 | 0.905445 | 0.019521379 | 0.2475 | 0.125685 |
| NaN | 0.5 | 0.2 | 0 | 0 | 70167 | 10 | 0 | 10 | 0.01 | 0.905445 | 0.019271105 | 0.2475 | 0.125685 |
| NaN | 0.5 | 0.2 | 0 | 0 | 70411.96346 | 10 | 0 | 10 | 0.01 | 1 | 0.012343455 | 0.044213426 | 0.053900803 |
| NaN | 0.5 | 0.2 | 0 | 0 | 16751.64683 | 10 | 0 | 10 | 0.01 | 1.011255 | 0.008784621 | 0.245085 | 0.069555 |
| NaN | 0.5 | 0.2 | 0 | 0 | 90617 | 10 | 0 | 10 | 0.01 | 0.705015 | 0.021273298 | 0.26193 | 0.195705 |
| NaN | 0.5 | 0.2 | 0 | 0 | 89337 | 10 | 0 | 10 | 0.01 | 0.705015 | 0.021273298 | 0.26193 | 0.195705 |
| NaN | 0.5 | 0.2 | 0 | 0 | 78145.19702 | 10 | 0 | 10 | 0.01 | 0.104676231 | 0.003169265 | 0.104676231 | 0.023161618 |
| NaN | 0.5 | 0.2 | 0 | 0 | 47841.08965 | 10 | 0 | 10 | 0.01 | 1 | 0.006338531 | 0.129050299 | 0.047752966 |
| NaN | 0.5 | 0.2 | 0 | 0 | 30836 | 10 | 0 | 10 | 0.01 | 0.776295 | 0.017268912 | 0.264945 | 0.16272 |
| NaN | 0.5 | 0.2 | 0 | 0 | 21002 | 10 | 0 | 10 | 0.01 | 0.776295 | 0.017519186 | 0.264945 | 0.16272 |
| NaN | 0.5 | 0.2 | 0 | 0 | 27365 | 10 | 0 | 10 | 0.01 | 0.805425 | 0.01526672 | 0.24909 | 0.162555 |
| NaN | 0.5 | 0.2 | 0 | 0 | 49666.40445 | 10 | 0 | 10 | 0.01 | 1 | 0.004003283 | 0.091827885 | 0.041748102 |
| NaN | 0.5 | 0.2 | 0 | 0 | 890589.2526 | 10 | 0 | 10 | 0.01 | 0.794775 | 0.019396242 | 0.245235 | 0.169035 |
| NaN | 0.5 | 0.2 | 0 | 0 | 54957.99837 | 10 | 0 | 10 | 0.01 | 0.758415 | 0.021323353 | 0.26121 | 0.17187 |
| NaN | 0.5 | 0.2 | 0 | 0 | 8224 | 10 | 0 | 10 | 0.01 | 0.680175 | 0.021023024 | 0.26193 | 0.21867 |
| NaN | 0.5 | 0.2 | 0 | 0 | 11394.89547 | 10 | 0 | 10 | 0.01 | 1 | 0.001000821 | 0.098441004 | 0.022589726 |
| NaN | 0.5 | 0.2 | 0 | 0 | 5261.328573 | 10 | 0 | 10 | 0.01 | 1 | 0.005838121 | 0.066886978 | 0.038459724 |
| NaN | 0.5 | 0.2 | 0 | 0 | 12104.01065 | 10 | 0 | 10 | 0.01 | 0.079546378 | 0.004503693 | 0.079546378 | 0.046323236 |
| NaN | 0.5 | 0.2 | 0 | 0 | 36039.67581 | 10 | 0 | 10 | 0.01 | 1 | 0.006838941 | 0.073689044 | 0.063194044 |
| NaN | 0.5 | 0.2 | 0 | 0 | 284445.6499 | 10 | 0 | 10 | 0.01 | 0.118469309 | 0.010008207 | 0.118469309 | 0.07992188 |

| Bulk Rock MnO Uncertainty | Bulk Rock MgO Uncertainty | Bulk Rock CaO Uncertainty | Bulk Rock Na2O Uncertainty | Bulk Rock K2O Uncertainty | Bulk Rock P2O5 Uncertainty | Analytical Water Uncertainty | Bulk Rock CO2 Uncertainty | Bulk Rock Cl Uncertainty | Bulk Rock B Uncertainty | Bulk Rock Sm Uncertainty | Bulk Rock Gd Uncertainty | Bulk Rock U Uncertainty | Bulk Rock Th Uncertainty |
|---|---|---|---|---|---|---|---|---|---|---|---|---|---|
| 0 | 0.08709 | 0.031335 | 0.06327 | 0.05019 | 0.00627 | 1 | 1 | 4 | 0 | 0 | 0 | 0.16 | 0.1 |
| 0 | 0.038115 | 0.016365 | 0.0633 | 0.069765 | 0.015075 | 1 | 1 | 4 | 0 | 0 | 0 | 0.16 | 0.1 |
| 0 | 0.038115 | 0.016365 | 0.0633 | 0.069765 | 0.015075 | 1 | 1 | 4 | 0 | 0 | 0 | 0.16 | 0.1 |
| 0.000129123 | 0.003482379 | 0.001119349 | 1 | 0.00807086 | 0 | 1 | 1 | 11.81672913 | 0 | 0.694666382 | 0.853206314 | 0.358072869 | 0.724832056 |
| 0.001878735 | 0.003465 | 0.013515 | 0.091785 | 0.040095 | 0.00801 | 1 | 1 | 12.51528374 | 0 | 0 | 0 | 0.18 | 0.1 |
| 0 | 0.14472 | 0.09054 | 0.0486 | 0.02235 | 0.010605 | 1 | 1 | 4 | 0 | 0 | 0 | 0.16 | 0.1 |
| 0 | 0.14472 | 0.09054 | 0.0486 | 0.02235 | 0.010605 | 1 | 1 | 4 | 0 | 0 | 0 | 0.16 | 0.1 |
| 0.000258245 | 0.002487414 | 0.002658454 | 0.050683622 | 0.031078833 | 0 | 1 | 1 | 8.315608956 | 0 | 0.798687776 | 0.926607101 | 1.110325904 | 0.993607628 |
| 0.000516491 | 0.005638138 | 0.006156421 | 1 | 0.017707707 | 0 | 1 | 1 | 8.115236003 | 0 | 0.882315915 | 1.00243233 | 0.428461694 | 0.339917675 |
| 0 | 0.09459 | 0.05526 | 0.076815 | 0.03771 | 0.010455 | 1 | 1 | 5 | 0 | 0 | 0 | 0.16 | 0.1 |
| 0 | 0.09459 | 0.05526 | 0.076815 | 0.03771 | 0.010455 | 1 | 1 | 5 | 0 | 0 | 0 | 0.16 | 0.1 |
| 0 | 0.09117 | 0.045105 | 0.078435 | 0.034185 | 0.00978 | 1 | 1 | 5 | 0 | 0 | 0 | 0.16 | 0.1 |
| 0.000258245 | 0.001658276 | 0.00209878 | 1 | 0.020598761 | 0 | 1 | 1 | 6.050627118 | 0 | 1.085377786 | 1.043511631 | 0.674925956 | 0.975697376 |
| 0.003718733 | 0.12441 | 0.028335 | 0.06414 | 0.035835 | 0.01845 | 1 | 1 | 51.62973554 | 0 | 0 | 0 | 0.16 | 0.08 |
| 0.003292628 | 0.116205 | 0.05829 | 0.06813 | 0.03957 | 0.00651 | 1 | 1 | 7.898972997 | 0 | 0 | 0 | 0.04 | 0.04 |
| 0 | 0.140925 | 0.08226 | 0.054195 | 0.029595 | 0.006315 | 1 | 1 | 5 | 0 | 0 | 0 | 0.16 | 0.1 |
| 0.000129123 | 0.000829138 | 0.000839512 | 1 | 0.015900798 | 0 | 1 | 1 | 4.878031826 | 0 | 0.729887456 | 1.075149501 | 0.902888206 | 0.510204393 |
| 0.000516491 | 0.006633103 | 0.003358048 | 1 | 0.011684678 | 0 | 1 | 1 | 4.317846986 | 0 | 1.359408291 | 1.232539484 | 1.750013439 | 0.929169193 |
| 0.000258245 | 0.011276275 | 0.005037071 | 0.050009638 | 0.020960143 | 0 | 1 | 1 | 1.651747969 | 0 | 0.641056741 | 0.742471355 | 0.885191554 | 0.993504182 |
| 0.000258245 | 0.003150724 | 0.001539105 | 1 | 0.011805138 | 0 | 1 | 1 | 3.848170259 | 0 | 0.607652754 | 0.332717498 | 0.421452242 | 0.390933818 |
| 0.000387368 | 0.002819069 | 0.010913655 | 0.047852888 | 0.038426929 | 0 | 1 | 1 | 31.37548563 | 0 | 0.774592739 | 0.241377728 | 1.140080894 | 0.984364403 |

| Bulk Rock Cr Uncertainty | Bulk Rock Li Uncertainty | Target K2O Uncertainty | Target CaO Uncertainty | Target TiO2 Uncertainty | Target Fe2O3 Uncertainty | Target Cl Uncertainty | Covariance |
|---|---|---|---|---|---|---|---|
| 2.4 | 0 | 1.022709478 | 0.017490082 | 0.182700088 | 0.780640677 | 4 | 0 |
| 1.2 | 0 | 1.485277723 | 0.004897223 | 0.195213792 | 0.343138759 | 4 | 0 |
| 1.2 | 0 | 1.525029682 | 0.005596826 | 0.192711051 | 0.368874166 | 4 | 0 |
| 0 | 0 | NaN | NaN | NaN | NaN | NaN | 0 |
| 0 | 0 | 0.590858656 | 0.00419762 | 0.10761786 | 0.537584056 | 12.51528374 | 0 |
| 6.6 | 0 | 0.592665563 | 0.267948054 | 0.212732979 | 0.726310373 | 4 | 0 |
| 6.6 | 0 | 0.61434845 | 0.27144607 | 0.212732979 | 0.714872415 | 4 | 0 |
| 0 | 0 | NaN | NaN | NaN | NaN | NaN | 0 |
| 0 | 0 | NaN | NaN | NaN | NaN | NaN | 0 |
| 2.8 | 0 | 0.91790886 | 0.009794446 | 0.172689124 | 0.905028477 | 5 | 0 |
| 2.8 | 0 | 0.932364118 | 0.009794446 | 0.175191865 | 0.867855111 | 5 | 0 |
| 1.8 | 0 | 0.86008783 | 0.030782544 | 0.152667197 | 0.913606946 | 5 | 0 |
| 0 | 0 | NaN | NaN | NaN | NaN | NaN | 0 |
| 4.4 | 0 | 0.91790886 | 0.030082941 | 0.100109637 | 0.709153435 | 51.62973554 | 0 |
| 1.8 | 0 | 0.968502262 | 0.050371436 | 0.165180901 | 0.889301284 | 7.898972997 | 0 |
| 2.2 | 0 | 0.780583913 | 0.161608356 | 0.210230238 | 1.026556788 | 5 | 0 |
| 0 | 0 | NaN | NaN | NaN | NaN | NaN | 0 |
| 0 | 0 | NaN | NaN | NaN | NaN | NaN | 0 |
| 0 | 0 | NaN | NaN | NaN | NaN | NaN | 0 |
| 0 | 0 | NaN | NaN | NaN | NaN | NaN | 0 |
| 0 | 0 | NaN | NaN | NaN | NaN | NaN | 0 |

**Supplementary Table 3. Full 36Cl output data. From CRONUS**
http://cronus.cosmogenicnuclides.rocks/2.0/html/cl/

| Sample Name | **Age (ka)** | Internal Uncertainty (ka) | Total Uncertainty (ka) | Erosion Rate | Scaling Ca Spallation | Scaling K Spallation | Scaling Fe Spallation | Scaling Ti Spallation | Scaling Cl Epithermal | Scaling Cl Thermal |
|---|---|---|---|---|---|---|---|---|---|---|
| AT-4125-250m | **60** | 4.7 | 10 | 0 | 4.4662 | 4.4662 | 4.4662 | 4.4662 | 4.4662 | 4.4662 |
| AT-3a1125-250m | **40.5** | 3.5 | 5.2 | 0 | 4.4662 | 4.4662 | 4.4662 | 4.4662 | 4.4662 | 4.4662 |
| AT-3a2250-500m | **38.5** | 3.5 | 5.2 | 0 | 4.4662 | 4.4662 | 4.4662 | 4.4662 | 4.4662 | 4.4662 |
| IT-10 | **29.5** | 1.7 | 5.7 | 0 | 4.5188 | 4.5188 | 4.5188 | 4.5188 | 4.5188 | 4.5188 |
| TAM-4 | **6** | 0.4 | 1 | 0 | 4.9507 | 4.9507 | 4.9507 | 4.9507 | 4.9507 | 4.9507 |
| TAM-51125-250m | **67** | 4.3 | 11 | 0 | 4.5985 | 4.5985 | 4.5985 | 4.5985 | 4.5985 | 4.5985 |
| TAM-52125-250m | **59.5** | 3.9 | 9.2 | 0 | 4.5985 | 4.5985 | 4.5985 | 4.5985 | 4.5985 | 4.5985 |
| TAM-6 | **26.1** | 1.3 | 4.4 | 0 | 4.9507 | 4.9507 | 4.9507 | 4.9507 | 4.9507 | 4.9507 |
| IRHZWE-12-11 | **17.2** | 0.9 | 3.6 | 0 | 4.9887 | 4.9887 | 4.9887 | 4.9887 | 4.9887 | 4.9887 |
| IRHZWE-61125-250m | **12.2** | 0.7 | 2.2 | 0 | 5.6633 | 5.6633 | 5.6633 | 5.6633 | 5.6633 | 5.6633 |
| IRHZWE-62125-250m | **5.82** | 0.3 | 0.84 | 0 | 5.6633 | 5.6633 | 5.6633 | 5.6633 | 5.6633 | 5.6633 |
| IRHZWE-4125-250m | **8.9** | 0.6 | 1.8 | 0 | 5.5727 | 5.5727 | 5.5727 | 5.5727 | 5.5727 | 5.5727 |
| IRHZWE-3 | **16.6** | 0.8 | 3.2 | 0 | 6.9845 | 6.9845 | 6.9845 | 6.9845 | 6.9845 | 6.9845 |
| AMEGUEDOUL-1 | **80** | 12.1 | 21 | 0 | 5.1435 | 5.1435 | 5.1435 | 5.1435 | 5.1435 | 5.1435 |
| A-12 | **4.4** | 0.9 | 1.1 | 0 | 4.4362 | 4.4362 | 4.4362 | 4.4362 | 4.4362 | 4.4362 |
| A-14125-250m | **1.05** | 0.2 | 0.26 | 0 | 4.4361 | 4.4361 | 4.4361 | 4.4361 | 4.4361 | 4.4361 |
| AM-11-11 | **7.2** | 0.6 | 1.5 | 0 | 3.8948 | 3.8948 | 3.8948 | 3.8948 | 3.8948 | 3.8948 |
| AM-8-11 | **2.7** | 0.9 | 1.1 | 0 | 4.162 | 4.162 | 4.162 | 4.162 | 4.162 | 4.162 |
| AM-9-11 | **13.2** | 0.7 | 2.5 | 0 | 4.22 | 4.22 | 4.22 | 4.22 | 4.22 | 4.22 |
| TOUBKAL-3 | **28.9** | 1.4 | 4.9 | 0 | 4.0716 | 4.0716 | 4.0716 | 4.0716 | 4.0716 | 4.0716 |
| TOUBKAL-4 | **50** | 4.9 | 11 | 0 | 3.8869 | 3.8869 | 3.8869 | 3.8869 | 3.8869 | 3.8869 |

| Scaling Fast Muons | Scaling Slow Muons | Production CA Spallation | Production K Spallation | Production Fe Spallation | Production Ti Spallation | Production CA Muons | Production K Muons | Production Cl Low Energy |
|---|---|---|---|---|---|---|---|---|
| 2.2567 | 2.2567 | 0.53203 | 35.1493 | 0.83675 | 0.15048 | 0.014214 | 0.9731 | 39.1904 |
| 2.2567 | 2.2567 | 0.14897 | 51.0472 | 0.3678 | 0.16079 | 0.0039933 | 1.4186 | 28.4275 |
| 2.2567 | 2.2567 | 0.17025 | 52.4135 | 0.39539 | 0.15873 | 0.0045646 | 1.4568 | 28.61 |
| 2.2755 | 2.2755 | 0.48535 | 12.5658 | 0.32672 | 0.17633 | 0.012891 | 0.34718 | 36.8627 |
| 2.4269 | 2.4269 | 0.14538 | 23.1219 | 0.65609 | 0.10093 | 0.0038006 | 0.63002 | 85.6466 |
| 2.3036 | 2.3036 | 8.6192 | 21.5403 | 0.82327 | 0.18529 | 0.22497 | 0.58233 | 31.0549 |
| 2.3036 | 2.3036 | 8.7318 | 22.3284 | 0.81031 | 0.18529 | 0.22791 | 0.60364 | 30.0293 |
| 2.4269 | 2.4269 | 0.39542 | 23.843 | 0.37961 | 0.11179 | 0.010241 | 0.64365 | 46.292 |
| 2.4402 | 2.4402 | 1.7314 | 10.6272 | 0.48568 | 0.1532 | 0.044531 | 0.28449 | 51.7264 |
| 2.6729 | 2.6729 | 0.36866 | 39.0364 | 1.2004 | 0.176 | 0.0090325 | 0.99974 | 73.7592 |
| 2.6729 | 2.6729 | 0.36866 | 39.6511 | 1.1511 | 0.17855 | 0.0090311 | 1.0153 | 68.1525 |
| 2.6418 | 2.6418 | 1.1441 | 36.1189 | 1.1965 | 0.15364 | 0.028268 | 0.93258 | 70.5075 |
| 3.1187 | 3.1187 | 0.47111 | 23.4606 | 0.45939 | 0.11606 | 0.010911 | 0.57308 | 65.1072 |
| 2.494 | 2.494 | 1.0713 | 36.933 | 0.88988 | 0.096531 | 0.027 | 0.9689 | 86.7583 |
| 2.2461 | 2.2461 | 1.4666 | 31.8603 | 0.91238 | 0.13022 | 0.038922 | 0.87492 | 32.6305 |
| 2.246 | 2.246 | 4.7053 | 25.6781 | 1.0532 | 0.16573 | 0.12451 | 0.70286 | 42.4449 |
| 2.0521 | 2.0521 | 0.16122 | 10.804 | 0.24014 | 0.026431 | 0.0045878 | 0.31737 | 27.0735 |
| 2.1482 | 2.1482 | 0.50454 | 7.5598 | 0.41161 | 0.13415 | 0.013859 | 0.21463 | 26.5616 |
| 2.169 | 2.169 | 0.92131 | 8.3485 | 0.24554 | 0.057108 | 0.025406 | 0.23836 | 19.9391 |
| 2.116 | 2.116 | 0.32352 | 11.1887 | 0.3542 | 0.087087 | 0.0088916 | 0.31844 | 21.8798 |
| 2.0494 | 2.0494 | 1.2346 | 24.2637 | 0.36738 | 0.11403 | 0.034583 | 0.70268 | 46.9575 |

| Sigma th | Sigma eth | Sigma sc | Qs | Qth | Qeth | Qmu | Cosmogenic Cl | Radiogenic Cl | Analytical (Internal) Uncertainty | Percent Ca | Percent K | Percent Cl |
|---|---|---|---|---|---|---|---|---|---|---|---|---|
| 0.0067341 | 0.029127 | 0.1156 | 0.95828 | 1.3722 | 1.1182 | 0.97165 | 4377502.303 | 163364.6973 | 4.7467 | 0.7108 | 47.01 | 51 |
| 0.0061688 | 0.029183 | 0.11469 | 0.95894 | 1.3788 | 1.1161 | 0.97161 | 3246017.529 | 112071.4712 | 3.5332 | 0.1875 | 64.32 | 34.85 |
| 0.0061615 | 0.029181 | 0.11467 | 0.95906 | 1.3789 | 1.1161 | 0.97161 | 3135043.855 | 112849.1448 | 3.5298 | 0.2101 | 64.74 | 34.38 |
| 0.0061928 | 0.029571 | 0.11487 | 0.98066 | 1.0844 | 1.0335 | 0.99451 | 1433964.517 | 41108.4831 | 1.7322 | 0.9812 | 25.43 | 72.6 |
| 0.0047638 | 0.029225 | 0.11373 | 0.95797 | 1.4011 | 1.1135 | 0.96987 | 573945.6038 | 391319.3962 | 0.35632 | 0.1352 | 21.53 | 77.65 |
| 0.0079388 | 0.02911 | 0.1171 | 0.96308 | 1.3592 | 1.12 | 0.97191 | 4071599.457 | 113320.5427 | 4.3026 | 14.03 | 35.1 | 49.27 |
| 0.0079348 | 0.02911 | 0.1171 | 0.96313 | 1.3593 | 1.12 | 0.9719 | 3610059.864 | 109598.1359 | 3.9345 | 14.24 | 36.45 | 47.73 |
| 0.0058274 | 0.028352 | 0.1134 | 0.96794 | 1.2922 | 1.0999 | 0.97765 | 1774073.619 | 22360.3813 | 1.254 | 0.566 | 34.16 | 64.59 |
| 0.0060317 | 0.029287 | 0.11574 | 0.95368 | 1.3841 | 1.1154 | 0.97004 | 1019381.933 | 123107.0671 | 0.92007 | 2.73 | 16.77 | 79.51 |
| 0.0067366 | 0.02913 | 0.11585 | 0.95792 | 1.371 | 1.1179 | 0.96775 | 1274126.742 | 258246.258 | 0.74029 | 0.3269 | 34.65 | 63.83 |
| 0.0067277 | 0.02913 | 0.11585 | 0.95791 | 1.3712 | 1.1179 | 0.96775 | 582038.8159 | 238724.1841 | 0.33382 | 0.3417 | 36.79 | 61.66 |
| 0.0062692 | 0.029129 | 0.11589 | 0.95873 | 1.3789 | 1.118 | 0.96806 | 902242.9167 | 254429.0833 | 0.63417 | 1.065 | 33.66 | 64.05 |
| 0.0055228 | 0.029267 | 0.11472 | 0.9576 | 1.3878 | 1.1134 | 0.96449 | 1356760.906 | 119409.0936 | 0.76621 | 0.5344 | 26.65 | 72.18 |
| 0.0075376 | 0.029333 | 0.11728 | 0.96014 | 1.3628 | 1.1173 | 0.96935 | 9552048.71 | 288804.2896 | 12.0794 | 0.8665 | 29.9 | 68.45 |
| 0.0067952 | 0.02922 | 0.11648 | 0.9593 | 1.3727 | 1.1182 | 0.97185 | 266263.3186 | 40188.6814 | 0.90973 | 2.217 | 48.2 | 48.05 |
| 0.00703 | 0.02907 | 0.11709 | 0.9606 | 1.3715 | 1.1212 | 0.97215 | 69695.2719 | 180555.7281 | 0.189 | 6.45 | 35.23 | 56.69 |
| 0.0051007 | 0.029259 | 0.11451 | 0.95998 | 1.4001 | 1.1138 | 0.97401 | 260594.6095 | 13594.3905 | 0.59752 | 0.4293 | 28.79 | 70.09 |
| 0.0057049 | 0.029323 | 0.11604 | 0.94842 | 1.3916 | 1.1154 | 0.97298 | 82362.1599 | 21894.8401 | 0.90705 | 1.464 | 21.96 | 75.03 |
| 0.0046506 | 0.029288 | 0.11499 | 0.95867 | 1.4106 | 1.1136 | 0.97282 | 355228.0014 | 24724.9986 | 0.67863 | 3.18 | 28.84 | 66.97 |
| 0.0056702 | 0.029568 | 0.11562 | 0.98613 | 1.0868 | 1.0338 | 0.99485 | 943199.1262 | 27733.8738 | 1.3855 | 0.9731 | 33.69 | 64.05 |
| 0.0065685 | 0.029456 | 0.11426 | 0.98959 | 1.0832 | 1.034 | 0.99501 | 3614282.231 | 33217.7695 | 4.9044 | 1.723 | 33.89 | 63.74 |